Application of deep learning method in web crippling strength prediction of cold-formed stainless steel channel sections under end-two-flange loading

Fang, Zhiyuan; Roy, Krishanu; Ma, Quincy; Uzzaman, Asraf; Lim, James B.P.

Published in:
Structures

DOI:
10.1016/j.istruc.2021.05.097

Published: 31/10/2021

Document Version
Peer reviewed version

Application of deep learning method in web crippling strength prediction of cold-formed stainless steel channel sections under end-two-flange loading

Zhiyuan Fang[a], Krishanu Roy[a,] *, Quincy Ma[a], Asraf Uzzaman[b], James B.P. Lim[a]

[a] Department of Civil and Environmental Engineering, The University of Auckland, New Zealand

[b] School of Computing, Engineering and Physical Sciences, University of the West of Scotland, United Kingdom

Abstract: This paper proposes a deep-learning framework, specifically, a deep belief network (DBN), for studying the web crippling performance of cold-formed stainless steel channel sections (lipped and unlipped as well as fastened and unfastened) with centered and offset web holes under the end-two-flange loading condition. G430 ferritic, S32205 duplex and 304 austenitic stainless steel grades are considered. A total of 17,281 data points for training the DBN are generated from an elasto plastic finite element model, validated from 69 experimental results reported in the literature. When a comparison was made against a further 53 experimental results reported in the literature, the DBN predictions were found to be conservative by around 10%. When compared with Backpropagation Neural Network (a typical shallow artificial neural network) and linear regression model based on PaddlePaddle, it was found that the proposed DBN outperformed these two methods, using the same big training data generated in this study. Using the DBN predictions, a parametric study is then conducted to investigate the effect of web holes, from which unified strength reduction factor equations are proposed. Finally, a reliability analysis is conducted, which shown that the

* Corresponding author at: Department of Civil and Environmental Engineering, The University of Auckland, New Zealand. Krishanu Roy, E-mail address: kroy405@aucklanduni.ac.nz

proposed equations can predict the web crippling strength of cold-formed stainless steel channel sections under the end-two-flange loading condition.

Keywords: Web crippling; Cold-formed steel; Deep learning; Stainless steel; Web hole; Finite element analysis.

1. Introduction

Stainless steel is a highly versatile material, possessing a unique selection of properties that can be exploited in structural (load bearing) applications. Cold-formed stainless steel (CFSS) channels are becoming increasingly popular as structural members due to its aesthetic appeal, and favorable material characteristics, particularly for resistance to heat and corrosion [1]. Web holes are often found in such sections for convenience of installation of services (see Fig.1). In the vicinity of the holes, however, localized failure in the web can occur, particularly under transverse concentrated loads. This research aims to study the web crippling strength of CFSS channel sections under the end-two-flange (ETF) loading condition.

Amongst all material grades of stainless steel, austenitic, ferritic and duplex grades are the most popular. It is well known that the stress-strain relationship of stainless steel differs from that of carbon steel, which is approximately linear up to the yield stress point. On the other hand, there is no clearly defined yield stress of stainless steel. Such a relationship is demonstrated in Appendix C of the American Society of Civil Engineers Specification (ASCE 8-02) [2]. In this paper, G430 ferritic, S32205 duplex and 304 austenitic stainless steel grades are considered.

Despite the popularity of stainless steels, there are very few studies concerned with web crippling of CFSS channel sections. In chronological order, Korvink et al. [3-4] conducted an experimental and numerical investigation on the web crippling strength of ferritic and austenitic CFSS channel sections; however, only one-flange loading conditions was considered. Bock et al. [5] conducted a numerical study on CFSS hollow and hat sections with ferritic CFSS channel sections; only the interior-one-flange (IOF) loading condition was considered. In terms of web holes, Yousefi et al. [6-10] recently conducted a series of web crippling tests on ferritic CFSS unlipped channel sections and proposed strength reduction factor equations for the reduced web crippling strength as a result of web holes; however, only ferritic CFSS was considered. For lipped channel sections, Yousefi et al. [11] described a numerical study covering ferritic, duplex, and austenitic CFSS; the results of 2,190 FE models were described. It should be noted that the DBN predictions described herein are based on 17,281 FE models and cover a wider range of parameters, thus allowing unified strength reduction factor equations to be proposed.

In terms of cold-formed carbon steel (CFCS) sections under web crippling, research is available in the literature. Keerthan and Mahendran [12] carried out an experimental study on plain channel beams with hollow flanges under two-flange loading condition. Sundararajah et al. [13] and Gunalan and Mahendran [14] considered the two-flange web crippling strength of CFCS lipped and unlipped channel sections using Direct Strength Method (DSM). Natario et al. [15] and Chen et al. [16] also considered CFCS sections.

For CFCS channel sections with web holes, research is available in the literature [17-27]. Uzzaman et al. [17-23] and Lian et al. [24-27] reported a number of studies, where they carried out experimental and numerical investigations and proposed web crippling reduction factor equations for CFCS channel sections with web holes under both one- and two-flange loading conditions.

Design guidance on web crippling performance has been summarized in ASCE 8-02 [2], AS/NZS 4673:2001 [28] and EC3 [29], which is a supplementary extension of EC3 [30] for carbon steel. However, when the web crippling strength predictions from these design standards were compared with test data available in the literature, it was found that the test-to-predicted ratio can vary from 0.95 to 1.40, indicating that in some cases they can be inaccurate by as much as 40% [6-11, 31-33]. Thus, there is a need for a comprehensive study on web crippling behaviour of CFSS channel sections with web holes.

Finite element analysis (FEA) is a useful and efficient research tool to predict the experimental web crippling strength of CFSS channel sections [9-14]. This paper investigates whether the numerical data, generated from a non-linear FE model, can be used to generate training data for Artificial Intelligence (AI) techniques, when predicting the experimental results from the literature.

Artificial Intelligence (AI) can be defined as the science and engineering of making intelligent computer programs and machines [34]. Shallow Artificial Neural Networks (ANN), a subset of AI, could be applied to investigate the structural performance of steel members accurately [35-39].–Gholizadeh et al. [35] used a shallow ANN, with training data from a non-linear FE model assessing the mechanical performance of steel beams. Dias and Silvestre [36] used a shallow ANN to do buckling analysis of tube sections under compression. Similarly, Tohidi and Sharifi [37] used a shallow ANN, with training data generated from non-linear elasto plastic FEA, to predict the compressive capacity of steel plate girder ends. Tahir and Mandal [38] also used a shallow ANN with Bayesian regularization backpropagation, with training data from experimental results, to estimate the compressive buckling load of thin cylindrical shells. In another relevant study, Abamberes et al. [39] adopted a shallow ANN, with training data generated from the non-linear elasto plastic FEA of the cellular beams and proposed equations for critical elastic buckling load of such beams. It should be noted that all the above-mentioned research studies used shallow ANN, and therefore they were limited in terms of modern AI techniques as they performed data regression and the predictions were based on limited data features, mostly relying on manual input, leading to some useful data being ignored.

Deep-learning method [40-43] in ANN is a useful technique to good data feature learning. Unlike shallow ANN, it can explore more useful data features from large data to make predictions with higher accuracy through building a network model with multiple hidden layers [44-45]. Structural performance of steel members can be investigated by using deep-learning methods [46-47]. Liu and Zhang [46] used a deep learning model, with training data from FEA, to provide an intelligent tool for rapid inspection of steel structural damage condition. Ali and Cha [47] proposed a method to detect hidden damage of steel members based on deep learning. In another study, Hung et al. [48] used a deep-learning method, with training data from nonlinear elasto plastic analysis. Similarly, Papazafeiropoulos et al. [49] used deep-learning method, with 2,200 training data, to predict the buckling coefficient of stiffened steel plate girders. From these, it was shown that the deep-learning method performs well in terms of data feature learning.

Deep Belief Network (DBN) [42-43] is a typical and effective deep-learning method composed of multiple Restricted Boltzmann Machine [50] layers and one layer of Backpropagation Neural Network (BPN) [51]. Generative model and back-propagation algorithm are used in the pretraining procedure for fine-tuning stage, respectively [45-43], which ensures the good ability of DBN to do data regression, and prediction work with a limited training sample [52-56]. DBN can be trained to represent the high-dimensional data features, while it is also a fast-learning algorithm to get optimal parameters. It has been proved that DBN is an effective method in structural analysis and damage identification of steel structures [56-57].

As mentioned previously, this paper intends to propose a new framework of DBN for studying the ETF structural performance of CFSS channel sections with centered and offset web holes. Three most popular stainless steel grades i.e. G430 ferritic, S32205 duplex and 304 austenitic stainless steel grades were used in this study. A total of 17,281 data points for training the DBN were generated from a validated elasto plastic FE model. The accuracy of the various methods was then calculated by evaluating the absolute percentage errors against the actual test data from the literature. The strength prediction accuracy of DBN was checked by comparing its results against the results of a BPN (a typical shallow ANN) and a Linear regression model based on the PaddlePaddle (Paddle model-a typical machine learning method) [58-62]. It was shown that the DBN predictions outperform the predictions of a shallow ANN and a typical machine learning method. Similarly, when the DBN predictions were compared with the design strengths calculated from the ASCE 8-02 [2], EC3 [30], and AISI&AS/NZS [63-64], it was found that the DBN has a better performance in predicting the web crippling strength of CFSS channel sections with web holes. Parametric effects on the web crippling strength of CFSS channel sections were also investigated. Based on the DBN output data, design recommendations in the form of strength reduction factors are proposed for web crippling strength of CFSS channel sections with web holes under ETF loading condition. Based on the data generated from DBN, a reliability analysis was performed, which shows that the proposed equations can closely predict the web crippling strength of cold-formed stainless steel channel sections with web holes.

2 Finite element analysis

In this study, ABAQUS 2019 [65] was used to develop a FE model for CFSS channel sections under ETF loading condition (see Fig.2). S4R shell elements were used to model the CFSS channel sections. The mesh sizes of 5 mm×5 mm and 10 mm×10 mm (length by width) was suitable for CFSS channel section and bearing plate, respectively. Mesh refinement was performed around web holes to achieve highly accurate results from the FEA. Finer mesh sizes were used near the rounded corners (see Fig.3).

2.1 Database construction

The constructed database contains the results of 17,281 FEA models. To create the database of training data, the following parameters were varied: depth of the web (d) from 140 mm to 300 mm; thickness of the channel (t) from 0.5 mm to 2.7 mm; ratio of flange width to web height (b_f/d) from 0.2 to 0.4; ratio of lip width to flange width (b_l/b_f) from 0.2 to 0.5; ratio of hole diameter to web flat depth (a/h) from 0.2 to 0.8; ratio of hole distance to web flat depth (x/h) from 0.23 to 0.64; ratio of bearing length to web flat depth (N/h) from 0.18 to 1.05.

2.2 Material property

Ferritic, duplex, and austenitic stainless-steel materials were selected to follow the requirements of ASCE 8-02 [2]. As a result, in this study, G430 ferritic stainless steel, S32205 duplex stainless steel and 304 austenitic stainless steel, were considered. The mechanical properties for each of the three grades considered, are listed in Table 1. In accordance with the ASCE 8-02 [2], the material stress-strain relationship basically follows equation 1 as given below:

$$\varepsilon = \begin{cases} \dfrac{f}{E} + 0.002\left(\dfrac{f}{f_{0.2}}\right)^n & f \le f_y \\ \dfrac{f - f_{0.2}}{E_{0.2}} + \left(\varepsilon_u - \varepsilon_{0.2} - \dfrac{f_u - f_{0.2}}{E_{0.2}}\right)\left(\dfrac{f - f_{0.2}}{f_u - f_{0.2}}\right)^m + \varepsilon_{0.2} & f_y \prec f \le f_u \end{cases} \quad (1)$$

Where,

$$E_{0.2} = \frac{E}{1 + 0.002n\dfrac{E}{f_{0.2}}} \quad (2)$$

For ferritic stainless steel, $\varepsilon_u = 0.6\left(1 - \dfrac{f_{0.2}}{f_u}\right)$ (3)

For duplex and austenitic stainless steel, $\varepsilon_u = 1 - \dfrac{f_{0.2}}{f_u}$ (4)

Where, E, $E_{0.2}$ is the Young's modulus and tangent modulus at 0.2% of proof stress; $f_{0.2}$, $f_{0.05}$ are 0.2% and 0.05% of proof stress; f_y, f_u are yield stress and ultimate stress; m and n are the strain hardening exponents, as shown in Table 1; ε_u is the ultimate strain.

2.3 Initial geometric imperfection and residual stresses

Geometric imperfection and residual stresses effects can be neglected in the web crippling studies which is already confirmed by numerous research studies [6-11 17-27]. Therefore, the initial geometric imperfection and residual stresses were not taken into consideration in FE modelling.

2.4 The Validation of FE model

The 69 experimental results of of Yousefi et al. [6-7] for stainless steel and Uzzaman et al. [18-19] for carbon steel were used for the validation purpose. The web crippling strengths obtained from the experimental tests [10-11, 22-23] and the FEA performed in this study, are shown in Table 2. As shown in Table 2, the average ratios of experimental to FEA strengths (F_{EXP}/F_{FEA}) are 1.08 and 1.00, respectively for the CFSS channel sections with un-fastened flanges and fastened flanges, and the values for CFCS are 1.02 and 0.94. Therefore, the FE models could closely predict the ETF web crippling strength of CFSS and CFCS channel sections with web holes.

3 Current design rules

Web crippling strength calculation procedure on CFCS channel sections is available in the current design standards including EC3 [30] and AISI&AS/NZS [63-64]. However, there are very few design rules available in the existing design standards ASCE 8-02 [2] and EC3 [29] for calculating web crippling strength of CFSS channel sections. Meanwhile, the effects of section geometry are not covered comprehensively in the equations of the design standards [2, 30, 63-64].

3.1 Design equations for web crippling strength of cold-formed steel channel sections without web holes

3.1.1 ASCE 8-02 [2]

ASCE 8-02 [2] provides a design equation on web crippling strength (P_{ASCE}) for CFSS channel sections. The coefficients (C_1, C_2, C_θ, C_t) are considered in the equations can be obtained by using the following equations:

$$P_{ASCE} = t^2 C_1 C_2 C_\theta C_t (244 - 0.57\frac{h}{t})(1 + 0.01\frac{N}{t}) \tag{5}$$

$$C_1 = \begin{cases} (1.33 - 0.33k)k & f_y/(66.5C_t) \le 1.0 \\ 1.34 & f_y/(66.5C_t) > 1.0 \end{cases} \tag{6}$$

$$C_2 = 1.15 - \frac{0.15r}{t} \le 1.0 \tag{7}$$

$$C_{\theta} = 0.7 + 0.3(\frac{\theta}{90})^2 \quad (8)$$

$$C_t = \begin{cases} 1.0 & \text{for US units} \\ 6.9 & \text{for SI units} \end{cases} \quad (9)$$

$$k = \frac{f_y}{33C_t} \quad (10)$$

Where, θ is the angle between the web plane and bearing surface.

3.1.2 AISI&AS/NZS [63-64]

The unified web crippling design equations of CFCS plain sections with different specific coefficients could be obtained from the AISI&AS/NZS [63-64]. The effect of fastened support was incorporated within the design rules of AISI&AS/NZS [63-64] for CFCS channel sections. The nominal web crippling strength ($P_{AISI\&AS/NZS}$) can be determined by Equation 11:

$$P_{AISI\&AS/NZS} = Ct^2 f_y \sin\theta (1 - C_w\sqrt{\frac{h}{t}})(1 - C_r\sqrt{\frac{r}{t}})(1 + C_l\sqrt{\frac{N}{t}}) \quad (11)$$

Where, C is a coefficient; l_b is the bearing length; C_r, C_l and C_w are the coefficients of inside bent radius, bearing length and web slenderness, respectively, and the values for the coefficients are shown in Table 3. It should be noted that these design equations are limited to the sections with r/t ratios lower than 1 and 12, respectively for un-fastened and fastened sections.

3.1.3 Eurocode 3 [30]

Eurocode 3 (EC3) [30] provides design equations for web crippling strength of CFCS plain channel sections under ETF and ITF loading conditions. However, these equations are complicated, when compared to the web crippling design equations given in AISI&AS/NZS [63-64]. Importantly, the same design equations are given for both the flange fastened and flange un-fastened support conditions, thus simply ignoring the change in web crippling strength due to flanges being fastened to the supports. These equations are limited for CFCS channel sections with $r/t \leq 6$ and $d_w/t \leq 200$. Equations (12) and (13) show the design formulas given in EC3 for ETF and ITF loading cases, respectively [30]:

$$P_{EC} = k_1 k_2 k_3 [6.66 - \frac{d_w / t}{64}][1 + 0.01\frac{N}{t}]t^2 f_y \tag{12}$$

$$P_{EC} = k_3 k_4 k_5 [21.0 - \frac{d_w / t}{16.3}][1 + 0.0013\frac{N}{t}]t^2 f_y \tag{13}$$

Where, d_w is the web height.

3.2 Design equations for web crippling strength of CFSS channels with web holes [6-7,11]

As mentioned in the introduction section, Yousefi et al. [6-7] proposed ETF web crippling strength reduction factor equations for ferritic CFSS unlipped channel sections with web holes. These equations were limited to $h/t \leq 157.68$, $N/t \leq 120.97$, $N/h \leq 1.15$, $a/h \leq 0.8$, and $\theta = 90°$. Strength reduction factor equations were also proposed for ferritic, duplex and austenitic CFSS lipped channel sections with web holes [11]. These equations were limited to $h/t \leq 156$, $N/t \leq 84$, $N/h \leq 0.63$, $a/h \leq 0.8$, and $\theta = 90°$.

In this paper, the results of DBN based on 17,281 FE models are used, from which unified equations are proposed. It should be noted that for offset holes, unlike the strength reduction equations of Yousefi et al. [11], the parameter *N/h* is included

4 Deep Belief Network (DBN)

4.1 Overview

As mentioned in the introduction section, DBN is a deep network model composed of multiple Restricted Boltzmann Machine [50] layers and one layer of Backpropagation Neural Network. In DBN, low-level features are converted to high-level and abstract representation attribute categories or features to explore distributed data feature representation [66]. DBN optimizes the initial values of network parameters in training process, which could avoid the trap of local optimal value due to random initialization parameters. Using multiple hidden layers with multiply-units could help to get more useful data features, however, direct training of multiply-layer network would lead to mis-convergence. Since layer-wise pre-training could avoid the mis-convergence caused by complexity of the model, the unsupervised layer-wise pre-training is to be used in DBN training process.

Denoising Auto Encoder (DAE) is an unsupervised neural network where training data is unlabeled. Data features obtained from the Denoising Auto Encoder (DAE) learning retain most of the information of input data, while the features are learned without adding label information. For supervised learning tasks such as regression prediction based on small amount of data, there is a strong correlation between the feature extraction and label information. Therefore, adding label information to output layer of Denoising Auto Encoder (DAE) can make the features obtained from the model more conducive to regression prediction. In this paper, in order to analyze more complicated data features, Stacked Denoising Auto Encoder (SDAE) was used. The training of SDAE can be subdivided into unsupervised layer-wise pre-training and supervised fine-tuning.

In terms of hyper-parameter optimization, Block Changing Grid Search (BCGS) is applied to optimize hyperparameter of DBN. The BCGS is based on Block Grid Search [67] by setting a variety of ranges for each hyperparameter. For the web crippling strength prediction, the Local Support Vector Machine (LSVM) [68] was applied.

4.2 Performance measures

The absolute percentage error (Err) for the i^{th} output, correlation coefficient (R^*), mean squared error (MSE) and the mean absolute error (MAE) were used to evaluate prediction performance of methods. The formulas for each parameter are given below:

$$\mathrm{Err}_i(\%) = \frac{|y_i - t_i|}{t_i} \times 100 \quad (14)$$

$$R^* = \frac{\sum_{i=1}^{n_d}(y_i - \overline{y_i})(t_i - \overline{t_i})}{\sqrt{\sum_{i=1}^{n_d}(y_i - \overline{y_i})^2 \sum_{i=1}^{n_d}(t_i - \overline{t_i})^2}} \quad (15)$$

$$\mathrm{MSE} = \frac{1}{n_d}\sum_{i=1}^{n_d}(t_i - y_i)^2 \quad (16)$$

$$\mathrm{MAE} = \frac{1}{n_d}\sum_{i=1}^{n_d}|y_i - t_i| \quad (17)$$

Where, t_i and y_i are the real and prediction output values for the i^{th} output, respectively. $\overline{t_i}$ and $\overline{y_i}$ are the average values of real and prediction outputs, respectively, and n_d is the number of data series.

4.3 Data training for web crippling strength prediction

The numerical data were generated from the validated FE models to develop the prediction models on web crippling strength of CFSS channel sections. According to Section 2.1 of this paper, before being normalized, the input (including 14 independent variables) and output for neural network are given as follows:

$$\mathrm{Input} = \left\{ b_w, b_l, b_f, r, t, L, N, a, x, m, n, n_h, h, E, \upsilon, f_y, f_u, \frac{r}{t}, \frac{N}{t}, \frac{h}{t}, \frac{b_l}{t}, \frac{a}{h}, \frac{x}{h}, \frac{N}{h} \right\} \quad (18)$$

$$\mathrm{Output} = \left\{ P_p \right\} \quad (19)$$

Where, L is the length of channel section, x denotes the hole distance to bearing block, and n_h

is the hole number. Finally, P_c and P_p are the web crippling strengths obtained from the training database and the predicted web crippling strengths, respectively. In order to properly train the data, the dependent variables were also used, which includes the ratio of section inside bend radius to web thickness (r/t), the ratio of bearing length to web thickness (N/t), the ratio of web flat depth to web thickness (h/t), the ratio of lip flat width to web thickness (b_l/t), the ratio of hole diameter to web flat depth (a/h), the ratio of hole distance to web flat depth (x/h), and the ratio of bearing length to web flat depth (N/h). Besides, the strengthen stage of stainless steel is considered as the strain hardening exponents (m, n) are included in input data variables.

To avoid over-fitting situation, early stopping technique for data analysis was used in this study. In this technique, the available data was divided into three groups: training, validation, and testing sets. Out of 17,281 data points for the prediction of Fc, 7,500 data points were used for training, 3,750 data for validation purpose and the remaining 3,750 data points for testing purpose. The training set was used for fitting the parameters (e.g. weights of connections between neurons in neural networks) of the model, and the fitted model was used to predict the responses of the observations within the validation set. Then, the testing set was used to provide an unbiased evaluation of a final model fit on the training dataset. Before the data analysis was performed, some low-performance data sets were deleted with the consideration of modelling error [69]. The number of neurons in the hidden layer of DBN was determined after several trial-and-error simulations. Training time for convergence was less than 60 minutes for 17,281 FEA data points. To speed up the learning process and obtain accurate results, input and output data series were normalized:

$$X_{si} = \frac{(X_i - \overline{X})}{(X_{\max} - X_{\min})} \tag{20}$$

Where, X_i is the value of ith variable, and $\overline{X}$ is the mean value of variables.

Input variables to the DBN were 19 independent CFSS channel section characteristics, while the P_c/P_p of CFSS channel section was the single output. The values of the ratio P_c/P_p, predicted from the DBN, are plotted in Fig.4. It is shown that R* values of DBN are equal to 0.99 for training, validation, and testing data set, respectively.

5 Comparison of deep-learning predictions with current design strengths

Prediction performance of the developed DBN, BPN and Paddle model are summarized and detailed in Table 4. In Table 5, the target parameters (R^*, MSE and MAE) are used to evaluate prediction performance of each model mentioned in this study. It can be observed from Table 4 that the deep-learning methods (the developed DBN and Paddle model) could provide highly accurate results when compared to the methods proposed in the current design standards of ASCE 8-02 [2], EC3 [30] and AISI&AS/NZS [63-64]. The best prediction performance values were obtained from the developed DBN for training (R^*=0.99, MSE=0.02, MAE=0.05), validation (R^*=0.99, MSE=0.02, MAE=0.06) and testing (R^*=0.99, MSE=0.02, MAE=0.08) data sets followed by Paddle model, BPN and design strengths. In Fig.5 and in Table 4, the average absolute percentage errors for sections with un-fastened flanges obtained from the FEA results, alongside the design strengths from the ASCE 8-02 [2], EC3 [30], AISI&AS/NZS [63-64], and the results obtained from the DBN, BPN and Paddle models are 7.1%, 8.2%,6.2%, 12.2%, 4.9%, 19.6 and 31.8%, respectively. Similarly, the values for sections with fastened flanges are 2.0%, 7.2%, 18.1%, 32.2%, 13.9%, 15.1%, and 15.1%. The results indicate that the design strengths as per the guidelines of ASCE 8-02

[2], EC3 [30] and AISI&AS/NZS [63-64] are comparatively lower than the FEA and DBN predictions by less than 10%. Both the FEA and DBN results have higher accuracy in predicting the the web crippling strength of CFSS channel sections with web holes.

6 Parametric study

Using the validated FE model and based on the DBN predictions, a detailed parametric study on the web crippling strength of CFSS channel sections was conducted.

6.1 Parametric study on the web crippling strength (P_n) of channel sections without web holes

Based on the studies available in the literature [6, 10-11], it can be confirmed that the web crippling strength of cold-formed stainless steel channel sections depends mainly on the ratio of section inside bend radius to web thickness (r/t), the ratio of bearing length to web thickness (N/t), and the ratio of web flat depth to web thickness (h/t). Therefore, a detailed investigation based on 2160 data was conducted.

6.1.1 Effect of r/t ratio on the web crippling strength (P_n)

The effect of r/t ratio on web crippling strength of cold-formed stainless steel channel sections with un-fastened and fastened flanges was studied based on 2160 data points. From Fig.6, it can be seen that r/t ratio has a negative influence on the web crippling strength of stainless steel channel sections. For cold-formed stainless steel channel sections with un-fastened flanges, when r/t ratio increased from 1 to 12, the web crippling strength of cold-formed ferritic, duplex, and austenitic grades of stainless steel channel sections decreased by 97.90%, 98.16% and 97.90%, respectively, despite the variation of r/t ratio from 1.3 to 3. Similar trend was observed for the same sections with fastened flanges, and the percentages are 97.57%, 97.79% and 97.57%, respectively, for the channel sections of ferritic, duplex, and austenitic grades of stainless steel.

6.1.2 Effect of N/t ratio on the web crippling strength (P_n)

Fig.7 shows the effect of *N*/*t* ratio on the web crippling strength. As the ratio (*N*/*t*) changed from 25 to 200, the web crippling strengths were reduced. From Fig.7, it can be seen that the reduced percentages of web crippling strengths for channel sections with un-fastened flanges are 96.91%, 97.27% and 96.89%, respectively for cold-formed ferritic, duplex, and austenitic grades of stainless steel, and the values for sections with fastened flanges are 96.19%, 96.65% and 96.21%.

6.1.3 Effect of h/t ratio on the web crippling strength (P_n)

Fig.8 shows the decreasing trend of web crippling strengths when the *h*/*t* ratio increased. With the increase of *h*/*t* ratio from 86.5 to 567, the average web crippling strengths of sections with un-fastened flanges are reduced by 97.69%, 98.13% and 97.67%, respectively for cold-formed ferritic, duplex, and austenitic grades of stainless steel, and the values of sections with fastened flanges are 97.18%, 97.69% and 97.20%.

6.1.4 Effect of fastened flanges on the web crippling strength (P_n)

From Figs.7-9, it can be concluded that the average web crippling strengths of sections with fastened flanges are higher than those with un-fastened flanges by 77.49%, 95.64% and 81.15%, respectively for cold-formed ferritic, duplex, and austenitic grades of stainless steel.

6.1.5 Effect of b_l/t ratio on the web crippling strength (P_n)

Figs.10(a) and 10(b) compare the web crippling strength (F_n) of unlipped and lipped channel sections with un-fastened and fastened flanges, respectively. From Figs.10(a) and

10(b), it can be seen that there is little difference between the values of F_n for unlipped and lipped sections with un-fastened flanges. While for sections with fastened flanges, the difference is big and the average ratios of F_n for lipped and unlipped channel sections are 1.096, 1.095 and 1.100, respectively for cold-formed ferritic, duplex, and austenitic grades of stainless steel. Therefore, it is necessary to consider the effects of lips on the web crippling strength of channel sections with fastened flanges.

From Fig.9(c), it can be observed that there is a downward trend for web crippling strength of sections with fastened flanges when the b_l/t ratio was increased. With the increase of b_l/t ratio from 4 to 61.5, the web crippling strengths for ferritic, duplex, and austenitic grades of stainless steel channels reduced by 95.78%, 96.67% and 95.85%, respectively. It should also be noted that the statistical relationship of b_l/t and P_n is nonlinear.

6.2 Hole effects on the web crippling strength reduction factor (R)

Based on the studies available in the literature [6, 10-11], it can be confirmed that the web crippling strength factors for cold-formed stainless steel channel sections depends mainly on the ratio of hole diameter to web flat depth (a/h), the ratio of hole distance to web flat depth (x/h), the ratio of bearing length to web flat depth (N/h) and on the effects of fasten flanges. Therefore, a detailed investigation based on 15,121 data was conducted.

6.2.1 Effect of a/h ratio on the web crippling strength reduction factor (R)

The effect a/h ratio on web crippling strength reduction factor (R) is shown in Fig.10 and in Table 6. From Fig.10, it can be seen that there is a downward trend of web crippling strength reduction factors with the increase in a/h ratio from 0.2 to 0.8. On the one hand, the web crippling strength reduction factors (R) for offset-hole sections with un-fastened and fastened flanges are similar, and the average web crippling strength reduction factors (*R*) for these two groups of sections are reduced from 0.95 to 0.65 and from 0.97 to 0.76, as the ratio *a*/*h* increased from 0.2 to 0.8. On the other hand, comparatively a bigger difference between the reduction factors (*R*) of centered-hole sections with un-fastened and fastened flanges. As shown in Table 6, the average web crippling strength reduction factors (*R*) for center-hole sections with un-fastened flanges decreased from 0.87 to 0.46. Similarly, the web crippling strength reduction factors (*R*) for sections with fastened flanges decreased from 0.89 to 0.51, when the *a*/*h* ratio changed from 0.2 to 0.8.

6.2.2 Effect of x/h ratio on the web crippling strength reduction factor (R)

With the *x*/*h* ratio increased from 0.09 to 0.60, the average reduction factors (*R*) for cold-formed ferritic stainless steel sections with un-fastened and fastened flanges changed from 0.94 to 0.67, and from 0.96 to 0.79, respectively. Similarly, the values of *R* changed from 0.95 to 0.67, and from 0.97 to 0.78 for cold-formed duplex stainless steel channel sections with un-fastened and fastened flanges, respectively. The values of *R* for cold-formed austenitic stainless steel sections with un-fastened and fastened flanges varied from 0.95 to 0.68, and from 0.97 to 0.79, respectively. In Fig.11, the change in web crippling strength reduction factor (*R*) with the change of *x*/*h* is shown, and this change follows the prediction of Equation 21 as given below:

$$\frac{\partial R}{\partial (x/h)} = k_{x/h} \quad (21)$$

Where $k_{x/h}$ is the related coefficient for the effect of *x*/*h* ratio on the web crippling strength reduction factor (*R*), and the value of $k_{x/h}$ can be found from Fig.11.

6.2.3 Effect of N/h ratio on the web crippling strength reduction factor (R)

When the N/h ratio increased from 0.18 to 1.05, the average strength reduction factors (R) for cold-formed ferritic stainless steel sections with un-fastened and fastened flanges, changed slightly by 4%, and 5% on average for each group of ratio a/h, respectively. Similarly, the values of R decreased both by 4% for cold-formed duplex stainless steel channel sections with un-fastened and fastened flanges, respectively. For cold-formed austenitic stainless steel sections with un-fastened and fastened flanges, the values of R increased by 4% and 5%, respectively. In Fig.12, the change in web crippling strength reduction factor (R) with the change of N/h ratio is shown, and this change follows the prediction of Equation 22 as given below:

$$\frac{\partial R}{\partial (N/h)} = k_{N/h} \tag{22}$$

Where, $k_{N/h}$ is the related coefficient for the effect of N/h ratio on the web crippling strength reduction factor (R), and the value of $k_{N/h}$ can be found from Fig.12.

6.2.4 Effect of fastened flanges on the web crippling strength reduction factor (R)

Fig.13 and Table 6 show the effect of fasten flanges on the web crippling strength reduction factor (R), with varying a/h ratio and hole position. From Table 6, there is a little difference on the average web crippling reduction factor (R) for different grades of stainless steel materials (Ferritic, Duplex and Austenitic). For sections with centered web holes, the average strength reduction factors (R) of channels with fastened flanges are higher than those with un-fastened flanges by 7.3%, and similarly the values for sections with offset web holes is 7.9%.

7 Proposed design equations

As mentioned previously, DBN could predict the web crippling strength of perforated

CFSS channels with higher accuracy when compared to the predictions of current standards at 50% to 90% and 5 to 20%, respectively for CFS sections with un-fastened flanges and sections with fastened flanges. Therefore, the results of DBN were used to propose design equations in the forms of web crippling strength and web crippling strength reduction factors. The limits for the proposed equations are $h/t \leq 600$, $N/t \leq 200$, $R/t \leq 12.0$, $N/h \leq 1.15$, $a/h \leq 0.8$ and $\theta = 90°$. Compared with the proposed equations by Yousefi et al. [6-7,11], the range of h/t has been extended. Besides, it should be noted that the design equations proposed in this paper are suitable for those cases where the friction coefficient between the loading block and the CFSS channel sections is in the range of 0.4 to 0.6, and the length of channel section should be followed:

$$L = k_L(1.5h + N) \tag{23}$$

Where, k_L is the coefficient and its values are suggested to be in between 0.95 and 1.10.

7.1 Design equations for cold-formed stainless steel channel sections without web holes

The design equations for web crippling strength (P_{prop}) of CFSS unlipped and lipped channel sections without web holes are proposed in this section. These equations are given below:

For sections with un-fastened flanges,

$$P_{prop} = Ct^2 f_y \sin\theta(1 - C_R\sqrt{\frac{r}{t}})(1 + C_N\sqrt{\frac{N}{t}})(1 - C_h\sqrt{\frac{h}{t}}) > 0 \tag{24}$$

For sections with fastened flanges,

$$P_{prop} = Ct^2 F_y \sin\theta(1 - C_R\sqrt{\frac{R}{t}})(1 + C_N\sqrt{\frac{N}{t}})(1 - C_h\sqrt{\frac{h}{t}})(1 + C_l\sqrt{\frac{b_l}{t}}) > 0 \tag{25}$$

Where, C is a coefficient (C_1 is for stainless steel with obvious stress hardening stage at stress-strain curve; C_2 is for stainless steel with not obvious stress hardening stage at stress-strain curve), θ is the angle between the plane of web and the plane of bearing surface, which is 90°, C_R is the inside bend radius coefficient, C_N is the bearing length coefficient, C_h is the web slenderness coefficient, and C_l is the lip slenderness coefficient. The effect of b_l/t is considered in the equations. The suggested values are shown in Table 7.

The prediction accuracy of the proposed equations was compared with the failure load from FEA as well as the current design standards. The proposed equations consider different kind of stainless steel, flange types and the effect of lip specifically. Table 8 shows that the proposed web crippling strength is very close to the numerical failure load from Yousefi et al. [6-7] and the database in this research, which confirms the accuracy of the design equations proposed in the current research. Besides, the prediction accuracy of proposed equations is higher than that of current design standards by around 10 to 50%.

7.2 Design equations for cold-formed stainless steel channel sections with web holes

The results of DBN were also used to propose design equations for CFSS unlipped and lipped channel sections with un-fastened flanges and fastened flanges. These design equations were developed in the form of web crippling strength reduction factors (R_{prop}), and the proposed equations are in relation to the terms of a/h, x/h, and N/h. Thus, the regression model for the equations can be shown in Equations 26 and 27 for sections with centered holes and offset holes:

For sections with centered hole,

$$R_{prop} = \alpha + \gamma \frac{a}{h} + \lambda \frac{N}{h} \leq 1 \qquad (26)$$

For sections with offset hole,

$$R_{prop} = \beta + \mu \frac{a}{h} + \zeta \frac{N}{h} + \xi \frac{x}{h} \leq 1 \quad (27)$$

Where, α, γ, λ, β, μ, ζ and ξ are equation coefficients. The detailed equation coefficient values for each type of sections with the material of ferritic, duplex, and austenitic stainless steel are summarized in Table 9. It is noted that the design equations cover the three kinds of stainless steel, fastened and unfastened flange type, as well as the effect of a/h, x/h and N/h on reduced web crippling strength.

The prediction accuracy of the proposed equations was compared with the failure loads obtained from the FFA and from the proposed equations of Yousefi et al. [6-7,11] and Uzzaman et al. [17-19]. Table 10 shows that the results obtained from the proposed reduction factors (R_{prop}) could closely predict the numerical failure load of Yousefi et al. [6-7] and the database in this research. Besides, it can be seen from Table 10 that the average values of R/R_{prop} (at 1.00 and 1.01 with COVs at 0.06 and 0.09 and for lipped sections with un-fastened and fastened flanges, respectively; at 0.98 and 0.95 with COVs at 0.03 and 0.02 and for unlipped sections with un-fastened and fastened flanges, respectively), which were predicted from the proposed equations are lower than the design strengths predicted by the proposed equations of Yousefi et al. [6-7,11] and Uzzaman et al. [17-19] with lower coefficient of variations (COVs), for unlipped and lipped sections with un-fastened and fastened flanges, respectively.

7.3 Reliability analysis

A comprehensive reliability analysis, using the method mentioned in Hsiao et al. [70] was conducted to evaluate the reliability of proposed design equations. As mentioned in the American standards (ASCE 8-02 [2] and AISI S100-16 [63]) and Australian/New Zealand

Standard (AS/NZS 4673:2001 [28]), any proposed design equation can be considered reliable when the reliability index (β) is greater than or equal to the target reliability index of 2.50 and 3.00, respectively. It is shown in Tables 11 and 12 that the values of β, predicted from the DBN results, in the case of cold-formed stainless steel unlipped and lipped channel sections with un-fastened and fastened flanges, are over the target reliability index of American standards [2,63] and Australian/New Zealand Standard [28]. This indicates that the proposed design equations can be used to determine the web crippling strength of CFSS unlipped and lipped channel sections with and without web holes with high degree of precision.

8 Conclusions

A framework of DBN is proposed for studying the structural performance of CFSS channel sections with web holes subjected to web crippling under end-two-flange. The three most popular stainless steel grades i.e. G430 grade of ferritic stainless steel, S32205 grade of duplex stainless steel and 304 grade of austenitic stainless steel was used in this study. A total of 17,281 data points for training the DBN are generated from a validated elasto plastic FE model. A comparison against 53 experimental results from the literature confirmed that the DBN predictions are conservative by 7% for sections with un-fastened flanges and 14% for sections with fastened flanges.

The accuracy of various methods including DBN, BPN, Paddle model, and the current standards was checked by evaluating the absolute percentage error against the actual test data available in the literature. The accuracy of the developed DBN was also compared with the accuracy of the typical prediction models (BPN and Paddle model). It was found that for some training data, the proposed DBN performed better than the typical models, with the average absolute percentage errors of 7% and 14% against the experimental results for CFSS sections with un-fastened flanges and fastened flanges, respectively. Similarly, the accuracy of the proposed DBN was checked by comparing its results with the design strengths calculated from the ASCE 8-02, EC3 and AISI&AS/NZS. The design strengths from the ASCE 8-02, EC3 and AISI&AS/NZS were inaccurate by 99.7%, 52.3% and 51.4% for channel sections with un-fastened flanges, and by 7.2%, 18.1% and 32.2% for those with fastened flanges, respectively.

Based on the DBN predicted results, new design equations in the form of web crippling strength reduction factors, were proposed for CFSS (ferritic, duplex, and austenitic) channel sections with un-fastened and fastened flanges under end-two-flange loading condition. The proposed design equations considered the effects of lip and plate elements on the web crippling strength of CFSS channel sections. Meanwhile, compared with the previous equations from the literature, the limitation range of proposed equations has been extended to $h/t \leq 600$, $N/t \leq 200$, $N/h \leq 1.15$, $a/h \leq 0.8$. Based on the data generated from DBN, a comprehensive reliability analysis was performed, which shows that the proposed equations can predict the web crippling strength of perforated CFSS channel sections with a high level of precision.

Acknowledgements

We thank the New Zealand eScience Infrastructure (NeSI, https://www.nesi.org.nz) and the data visualization lab in The university of Auckland for providing us with high-performance calculating and computing machines.

References

[1] N. Baddoo, Designing structural stainless steel members to Eurocode 3, NEW Steel Constr. (April, 2009) 30-32.

[2] American Society of Civil Engineers (ASCE), Specification for the Design of Cold-formed Stainless Steel Structural Members, SEI/ASCE 8-02, Reston, Va, 2002.

[3] S.A. Korvink, G.J. van den Berg, Web crippling of stainless steel cold-formed beams. Proc., 12th Int. Specialty Conf. On Cold-Formed Steel Structures, University of Missouri-Rolla, St. Louis, 1994, pp. 551–569.

[4] S.A. Korvink, G.J. van den Berg, P. van der Merwe, Web crippling of stainless steel cold-formed beams, J. Constr. Steel Res. 34 (1995) 225–248.

[5] M. Bock, I. Arrayago, E. Real, E. Mirambell, Study of web crippling in ferritic stainless steel cold formed sections. Thin-Walled Struct. 69 (2013) 29–44.

[6] A. M. Yousefi, J. B. P. Lim, G. Charles Clifton, Web bearing capacity of unlipped cold-formed ferritic stainless steel channels with perforated web subject to end-two-flange (ETF) loading. Eng. Struct. 152 (2017) 804–818.

[7] A. M. Yousefi, J. B. P. Lim, G. Charles Clifton, Web crippling design of cold-formed ferritic stainless steel unlipped channels with fastened flanges under end-two-flange loading condition, J. Constr. Steel Res. (2017).

[8] A. M. Yousefi, J. B. P. Lim, G. Charles Clifton, Cold-formed ferritic stainless steel unlipped channels with web openings subjected to web crippling under interior-two-flange loading condition – Part I: Tests and finite element model validation. Thin-Walled Struct. 116 (2017) 333–341.

[9] A. M. Yousefi, J. B. P. Lim, G. Charles Clifton, Web Crippling Behavior of Unlipped Cold-Formed Ferritic Stainless Steel Channels Subject to One-Flange Loadings. J Struct Eng. 144 (8) (2018) 04018105.

[10] A. M. Yousefi, J. B. P. Lim, G. Charles Clifton, Web crippling strength of perforated cold-formed ferritic stainless steel unlipped channels with restrained flanges under one-flange loadings. Thin-Walled Struct. 137 (2019) 94–105.

[11] A. M. Yousefi, A. Uzzaman, J. B. P. Lim, G. C. Clifton, B. Young, Web crippling strength of cold-formed stainless-steel lipped channels with web perforations under end-two-flange loading. Adv. Struct. Eng. 20 (2) (2017) 1845–1863.

[12] K. Poologanathan, M. Mahendran, E. Steau, Experimental study of web crippling behaviour of hollow flange channel beams under two flange load cases, Thin-Walled Struct. 85 (2014) 207-219.

[13] L. Sundararajah, M. Mahendran, P. Keerthan, Experimental studies of lipped channel beams subject to web crippling under two-flange load cases, J. Struct. Eng. 142 (2016) 04016058.

[14] S. Gunalan, M. Mahendran, Web crippling tests of cold-formed steel channels under two flange load cases, J. Constr. Steel Res. 110 (2015) 1-15.

[15] P. Natário, N. Silvestre, D. Camotim, Computational modelling of flange crushing in coldformed steel sections, Thin-Walled Struct. 84 (2014) 393-405.

[16] Y. Chen, X. Chen, C. Wang, Experimental and finite element analysis research on coldformed steel lipped channel beams under web crippling, Thin-Walled Struct. 87 (2015) 41-52.

[17] A. Uzzaman, J.B.P. Lim, D. Nash, J. Rhodes, B. Young, Web crippling behaviour of cold-formed steel channel sections with offset web holes subjected to interior two flange loading, Thin-Walled Struct. 50 (2012) 76–86.

[18] A. Uzzaman, J.B.P. Lim, D. Nash, J. Rhodes, B. Young, Cold-formed steel sections with web openings subjected to web crippling under two-flange loading conditions—Part I: tests and finite element analysis, Thin-Walled Struct. 56 (2012) 38–48.

[19] A. Uzzaman, J.B.P. Lim, D. Nash, J. Rhodes, B. Young, Cold-formed steel sections with web openings subjected to web crippling under two-flange loading conditions—Part II: parametric study and proposed design equations, Thin-Walled Struct. 56 (2012) 79–87.

[20] A. Uzzaman, J.B.P. Lim, D. Nash, J. Rhodes, B. Young, Effect of offset web holes on web crippling strength of cold-formed steel channel sections under end-two-flange loading condition, Thin-Walled Struct. 65 (2013) 34–48.

[21] A. Uzzaman, J.B.P. Lim, D. Nash, B. Young, Effects of edge-stiffened circular web openings on the web crippling strength of cold-formed steel channel beams under one-flange loading conditions, Eng. Struct. 139 (2017) 96-107.

[22] A. Uzzaman, J.B.P. Lim, D. Nash, K. Roy, Cold-formed steel channel beams under end-two-flange loading condition: Design for edge-stiffened holes, unstiffened holes and plain webs, Thin-Walled Struct. 147(2020) 106532.

[23] A. Uzzaman, J.B.P. Lim, D. Nash, K. Roy, Web crippling behaviour of cold-formed steel channel sections with edge-stiffened and unstiffened circular holes under interior-two-flange loading condition, Thin-Walled Struct. 154 (2020) 106813.

[24] Y. Lian, A. Uzzaman, J.B.P. Lim, G. Abdelal, D. Nash, B. Young, Effect of web holes on web crippling strength of cold-formed steel channel sections under end-oneflange loading condition – Part I: tests and fnite element analysis, Thin-Walled Struct. 107 (2016) 443–452.

[25] Y. Lian, A. Uzzaman, J.B.P. Lim, G. Abdelal, D. Nash, B. Young, Effect of web holes on web crippling strength of cold-formed steel channel sections under end-oneflange loading condition - Part II: parametric study and proposed design equations, Thin-Walled Struct. 107 (2016) 489–501.

[26] Y. Lian, A. Uzzaman, J.B.P. Lim, G. Abdelal, D. Nash, B. Young, Web crippling behaviour of cold-formed steel channel sections with web holes subjected to interior-one-flange loading condition-Part I: experimental and numerical investigation, Thin-Walled Struct. 111 (2017) 103–112.

[27] Y. Lian, A. Uzzaman, J.B.P. Lim, G. Abdelal, D. Nash, B. Young, Web crippling behaviour of cold-formed steel channel sections with web holes subjected to interior-one-flange loading condition – Part II: parametric study and proposed design equations, Thin-Walled Struct. 114 (2017) 92–106.

[28] Australian/New Zealand Standard (AS/NZS), Cold-Formed Stainless Steel Structures, AS/NZS 4673:2001, Standards Australia, Sydney, Australia, 2001.

[29] Eurocode 3: Design of steel structures—Part 1.4 (EN 1993-1-4). General rules—Supplementary rules for stainless steels. European Committee for Standardization (CEN), Brussel; 2006.

[30] Eurocode 3: Design of steel structures—Part 1.3 (EN 1993-1-3). General rules—Supplementary rules for cold-formed members and sheeting. European Committee for Standardization (CEN), Brussel; 2006.

[31] F. Zhou, B. Young, Cold-Formed Stainless Steel Sections Subjected to Web Crippling. J Struct Eng. 132(1) (2006) 134–144.

[32] F. Zhou, B. Young, Cold-Formed High-Strength Stainless Steel Tubular Sections Subjected to Web Crippling. J Struct Eng. 133 (3) (2007) 368–377.

[33] F. Zhou, B. Young, Web Crippling of Cold-Formed Stainless Steel Tubular Sections. Adv. Struct. Eng. 11(6) (2008) 679–691.

[34] McCharty J What is artificial intelligence? Technical report, Computer Science Department, Stanford University, (2007).

[35] S. Gholizadeh, A. Pirmoz, R. Attarnejad, Assessment of load carrying capacity of castellated steel beams by neural networks, J. Constr. Steel Res. 67 (5) (2011) 770-779.

[36]. J.L.R. Dias, N. Silvestre, A neural network based closed-form solution for the distortional buckling of elliptical tubes, Eng. Struct. 33(6) (2011) 2015–2024.

[37] S. Tohidi, Y. Sharifi, Load-carrying capacity of locally corroded steel plate girder ends using artificial neural network, Thin-Walled Struct. 100 (2016) 48–61.

[38] Z. ul R. Tahir, P. Mandal, Artificial neural network prediction of buckling load of thin cylindrical shells under axial compression, Eng. Struct. 152 (2017) 843-855.

[39] M. Abambres, K. Rajana, K. Tsavdaridis, T. Ribeiro, Neural network-based formula for the buckling load prediction of I-section cellular steel beams, Comp. 8(1) (2018) 2.

[40] X. Qiu, Y. Ren, P.N. Suganthan, G.A.J. Amaratunga, Empirical mode decomposition based ensemble deep learning for load demand time series forecasting, Appl. Soft Comput. 54 (2017) 246-255.

[41] H. Wang, G. Li, G. Wang, J. Peng, H. Jiang, Y. Liu, Deep learning based ensemble approach for probabilistic wind power forecasting. Appl. Energy. 188 (2017) 56-70.

[42] G.E. Hinton, Reducing the dimensionality of data with neural networks, Sci., 313 (5786) (2006) 504-507.

[43] Y. Bengio, P. Lamblin, D. Popovici, H. Larochelle, Greedy layerwise training of deep networks, Proceedings of 20th Annual Conference on Neural Information Processing Systems. Vancouver: Neural information processing system foundation. (2007) 153-160.

[44] C. Li, Z. Ding, J. Yi, Y. Lv, G. Zhang, Deep belief network based hybrid model for building energy consumption prediction, Energies. 11 (1) (2018) 242.

[45] W. Huang, G. Song, H. Hong, K. Xie, Deep architecture for traffic flow prediction: deep belief networks with multitask learning, IEEE. T. Intell. Transp. Syst. 15(5) (2014) 2191-2201.

[46] H. Liu, Y. Zhang, Image-driven structural steel damage condition assessment method using deep learning algorithm. Meas, 133 (2019) 168-181.

[47] R. Ali, Y.-J. Cha, Subsurface damage detection of a steel bridge using deep learning and uncooled micro-bolometer. Constr Build Mater. 226 (2019) 376-387.

[48] T. V. Hung, V. Q. Viet, D. V. Thuat, A deep learning-based procedure for estimation of ultimate load carrying of steel trusses using advanced analysis, J. Sci. Technol. Civ. Eng. 13 (3) (2019) 113-123.

[49] G. Papazafeiropoulos, QV. Vu, VH. Truong, MC. Luong, VT. Pham, Prediction of buckling coefficient of stiffened plate girders using deep learning algorithm. In: C. Ha-Minh, D. Dao, F. Benboudjema, S. Derrible, D. Huynh, A. Tang, (eds) CIGOS 2019, Innovation for Sustainable Infrastructure. Lecture Notes in Civil Engineering, vol 54 (2020). Springer, Singapore.

[50] P. Smolensky, Information processing in dynamical systems: foundations of harmony theory, parallel distributed processing, D.E. Rumelhart and J.L. McClelland, eds., vol. 1, chapter 6, pp. 194-281, MIT Press, 1986.

[51] I. Goodfellow, Y. Bengio, A. Courville, Back-propagation and other differentiation algorithms. In Deep Learning, MIT Press: Cambridge, MA, USA, 2016; pp. 200-220.

[52] H. Xu, C. Jiang, Deep belief network-based support vector regression method for traffic flow forecasting. Neural Comput & Applic 32 (2020) 2027-2036.

[53] A. S. Qureshi, A. Khan, A. Zameer, A. Usman, Wind power prediction using deep neural network based meta regression and transfer learning, Appl. Soft Comput. 58 (2017) 742-755.

[54] X. Qiu, Y. Ren, P.N. Suganthan, G.A.J. Amaratunga, Empirical mode decomposition based ensemble deep learning for load demand time series forecasting, Appl. Soft Comput. 54 (2017) 246-255.

[55] H. Wang, G. Li, G. Wang, J. Peng, H. Jiang, Y. Liu, Deep learning based ensemble approach for probabilistic wind power forecasting. Appl. Energy. 188 (2017) 56-70.

[56] G. Fan, J. Li, H. Hao, Vibration signal denoising for structural health monitoring by residual convolutional neural networks. Meas. 1 (2020) 107651.

[57] Z. Ding, J. Li, H. Hao, Structural damage identification by sparse deep belief network using uncertain and limited data. Struct. Control. Health Monit. 21 (2020) 18-22.

[58] Y. Ma, D. Yu, T. Wu, H. Wang, PaddlePaddle: An open-source deep learning platform from industrial practice, Front. Comput. Sci. 1 (1) (2019) 105-115.

[59] B. Company, PaddlePaddle-based AI, [Online]. Available: http://en.paddlepaddle.org/.

[60] B. Zhao, H. Xiong, J. Bian, Z. Guo, C. Xu, D. Dou, COMO: Widening deep neural networks with convolutional maxout. IEEE T. Multimed. (2020) 1-1.

[61] X. Wang, X. Li, J. Yu, M. Sun, P. Li, Improved touch-screen inputting using sequence-level prediction generation, (2020) 3077-3083.

[62] Z. Hu, Research and implementation of railway technical specification question answering system based on deep learning, 2020 IEEE 5th Information Technology and Mechatronics Engineering Conference (ITOEC), Chongqing, China, 2020, pp. 5-9.

[63] American Iron and Steel Institute (AISI). North American Specification for the Design of Cold-formed Steel Structural Members AISI S100-16; 2016.

[64] Australia/New Zealand Standard (AS/NZS). Cold-Formed Steel Structures, AS/NZS 4600:2018. Standards Australia/ Standards New Zealand; 2018.

[65] ABAQUS Analysis User's Manual-Version 6.14-2, ABAQUS Inc., USA, 2018.

[66] H.W. Ian, F. F. Eibe, A. H. Mark, J. P. Christopher, Data mining (Fourth Edition), New Zealand, 2017.

[67] X. Jing, L.-P. Chau, An Efficient Three-Step Search Algorithm for Block Motion Estimation. IEEE Trans. Multimedia. 6 (3) (2004) 435-438.

[68] V.L. Brailovsky, O. Barzilay, R. ShahaveR, On global, local, mixed and neighborhood kernels for support vector machines, Pattern. Recognit. Lett. 20 (11-130) (1999) 1183-1190.

[69] R. P. Rokade, K. Balaji Rao, B. Palani, Determination of Modelling Error Statistics for Cold-Formed Steel Columns, Adv. Civ. Eng. (2020) 1-25.

[70] L. Hsiao, W. Yu, T.V. Galambos, Load and resistance factor design of cold formed steel, calibration of the AISI design provisions, Ninth Progress Report, Civil Engineering Study 88-2, University of Missouri-Rolla, Rolla, Missouri, U.S.A., February 1988.

Notation

a	Hole diameter;
a/h	Hole diameter to web flat depth;
b_f	Overall flange width of section;
b_l	Lip flat width;
b_l/t	Ratio of lip to thickness;
c_1	Width of top lip;
c_2	Width of bottom lip;
C, C_1, C_2, C_θ, C_t	Coefficients from ASCE 8-02 [6];
Cov	Coefficient of variation;
DBN	Deep Belief Network;
d	Overall web depth of section;
d_w	Web height between flange mid-lines;
d/b_f	Ratio of web to flange;
d/b_l	Ratio of web to lip;
e_0	Member imperfection magnitude;
E	Young’s modulus;
Err	Absolute percentage error;
$E_{0.2}$	Tangent modulus at 0.2% of proof stress;

EOF	End-one-flange loading condition;
ETF	End-two-flange loading condition;
f_u	Ultimate material tensile strength;
f_y	Material yield stress;
$f_{0.2}$	0.2% of proof stress;
$f_{0.05}$	0.05% of proof stress;
FEA	Finite element analysis;
h	Depth of the flat portion of web;
h/t	Web flat depth to web thickness;
IOF	Interior-one-flange loading condition;
ITF	Interior-two-flange loading condition;
k_1,k_2,k_3,k_4,k_5	Coefficients from EC3 [39];
k_L	Coefficient from the length control equation;
L	Length of channel section;
m, n	Strain hardening exponents;
MAE	Mean absolute error;
MSE	Mean squared error;
n_d	Number of data series;
n_h	Hole number;
N	Bearing length;
N/h	Bearing length to web flat depth;
N/t	Bearing length to web thickness;
P_{A0}	Web crippling strength of sections without holes;
$P_{\mathrm{AISI\&AS/NZS}}$	Predicted web crippling strength of cold-formed stainless steel channel section from AISI S100-16 and AS/NZS 4600:2018;
P_{DBN}	Predicted web crippling strength of cold-formed stainless steel channel section from DBN;

P_{EXP}	Web crippling strength from experiments;
P_{FEA}	Web crippling strength from the finite element analysis;
P_c	Web crippling strength value from the training database;
P_p	Predicted web crippling strength value;
P_{prop}	Web crippling strength from proposed equations;
P_w	Web crippling strength with web holes from Yousefi et al. [6-7];
r	Inside bend radius;
r/t	Section inside bend radius to web thickness;
R	Web crippling strength reduction factor;
R^*	Correlation coefficient;
R_{DBN}	Reduction factor from DBN output;
R_{prop}	Reduction factor from proposed equations;
R_{Yousefi}	Reduction factor from Yousefi et al. [6-7];
t	Section/web thickness;
x	Hole distance to bearing block;
x/h	Hole distance to web flat depth;
X_i	Value of variables of input vectors;
$\overline{X}$	Mean value of variables of input vectors;
υ	Passion ratio;
$\upsilon_{\mathrm{elastic}}$	Poisson ratio at elastic stage;
$\upsilon_{\mathrm{plastic}}$	Poisson ratio at plastic stage
$\sigma_{0.05}$	0.05% proof stress;
ε_u	Ultimate strain;
γ_{M1}	Partial safety factor;
α, γ, λ, ρ, μ, ζ	Equation coefficients from Yousefi et al. [15];

List of tables

Table 10 Comparison of proposed equations for web crippling strength reduction factor with other calculation methods

(a) For sections with un-fastened flanges

(b) For sections with fastened flanges

Table 11 Comparison of DBN output data with the proposed web crippling strength of cold-formed stainless steel channel section

(a) With un-fastened flanges

(b) With fastened flanges

Table 12 Comparison of DBN output data with the proposed web crippling strength reduction factor of cold-formed stainless steel channel section

(a) With un-fastened flanges and center web hole

(b) With un-fastened flanges and offset web hole

(c) With fastened flanges and center web hole

(d) With fastened flanges and offset web hole

Table 1 Material property summary

Index \ Material	Ferritic stainless steel		Duplex stainless steel	Austenitic stainless steel
	G430		S32205	304
f_y (MPa)	205	284	450	205
f_u (MPa)	450	462	655	515
E (GPa)	200		200	193
m	2.5	3.03	3.27	2.31
n	14		8	7

Table 2 Comparison of experimental results and FEA results of sections from the literature [10-11, 22-23]

(a) Sections with un-fastened flanges

Specimen ID	Web	Flange	Lip	Bend radius	Thickness	Hole dia	Bearing length	Yield stress	Material	Exp.load	FEA result	P_{EXP}/P_{FEA}
	d	b_f	b_l	r	t	a	N	f_y		P_{EXP}	P_{FEA}	
	(mm)	(mm)	(mm)	(mm)	(mm)	(mm)	(mm)	(MPa)		(kN)	(kN)	
1	178.54	60.10	0	1.21	1.17	0	50	284	Stainless steel	1.51	1.47	1.03
2	178.56	60.12	0	1.20	1.14	68.77	50	284	Stainless steel	0.99	0.97	1.03
3	178.29	60.20	0	1.19	1.16	68.83	50	284	Stainless steel	1.29	1.25	1.03
4	178.15	60.07	0	1.20	1.14	0	75	284	Stainless steel	1.63	1.55	1.05
5	178.12	60.11	0	1.20	1.18	68.76	75	284	Stainless steel	1.25	1.21	1.03
6	178.4	60.17	0	1.20	1.15	68.95	75	284	Stainless steel	1.43	1.40	1.02
7	178.34	60.16	0	1.20	1.13	0	100	284	Stainless steel	1.76	1.69	1.04
8	178.46	60.04	0	1.20	1.15	68.86	100	284	Stainless steel	1.33	1.26	1.05
9	178.49	60.05	0	1.20	1.14	68.88	100	284	Stainless steel	1.57	1.54	1.02
10	203.54	75.02	0	1.21	1.17	0	50	284	Stainless steel	1.39	1.30	1.07
11	203.58	74.96	0	1.20	1.19	78.8	50	284	Stainless steel	0.97	0.94	1.03
12	203.57	74.98	0	1.19	1.16	78.85	50	284	Stainless steel	1.16	1.10	1.06
13	203.56	75.00	0	1.21	1.17	0	75	284	Stainless steel	1.44	1.45	0.99
14	203.37	74.98	0	1.20	1.00	78.81	75	284	Stainless steel	0.99	0.66	1.50
15	203.49	74.96	0	1.20	1.14	78.84	75	284	Stainless steel	1.23	1.18	1.04
16	203.76	75.02	0	1.20	1.12	0	100	284	Stainless steel	1.51	1.42	1.07
17	203.64	74.94	0	1.20	1.13	78.86	100	284	Stainless steel	1.09	1.04	1.05
18	203.68	75.01	0	1.20	1.11	78.84	100	284	Stainless steel	1.29	1.22	1.06
19	253.47	100.02	0	1.20	1.19	0	50	284	Stainless steel	1.14	1.10	1.03
20	253.52	100.00	0	1.21	1.23	92.1	50	284	Stainless steel	0.9	0.87	1.04

21	253.54	99.98	0	1.20	1.18	92.22	50	284	Stainless steel	1.01	0.94	1.07
22	253.54	100.00	0	1.20	1.20	0	75	284	Stainless steel	1.31	1.24	1.06
23	253.47	99.97	0	1.20	1.20	98.88	75	284	Stainless steel	0.95	0.87	1.10
24	254.57	99.99	0	1.20	1.15	98.75	75	284	Stainless steel	1.02	0.95	1.08
25	253.59	100.02	0	1.20	1.18	0	100	284	Stainless steel	1.4	1.28	1.09
26	253.64	99.95	0	1.20	1.08	98.8	100	284	Stainless steel	0.97	0.71	1.38
27	253.51	100.00	0	1.20	1.14	98.87	100	284	Stainless steel	1.08	1.02	1.06
Average												1.08
Cov												0.11
28	142.2	58.6	15.9	4.8	1.23	0	90	455	Carbon steel	2.21	2.04	1.08
29	142.2	58.6	15.9	4.8	1.23	27.9	90	455	Carbon steel	1.98	2.11	0.94
30	141.8	58.9	15.6	4.8	1.24	0	90	455	Carbon steel	2.35	2.32	1.01
31	202.1	63.1	17.5	5	1.45	0	90	455	Carbon steel	2.7	2.52	1.07
32	202.1	63.1	17.5	5	1.45	0	90	455	Carbon steel	2.84	2.77	1.03
33	263.4	63.4	14.4	5.5	1.56	0	120	455	Carbon steel	2.55	2.35	1.09
34	263.4	63.4	14.4	5.5	1.56	51.8	120	455	Carbon steel	2.29	2.31	0.99
35	262.8	63.4	14.7	5.5	1.55	103.4	120	455	Carbon steel	1.77	1.87	0.95
36	262.8	63.4	14.7	5.5	1.55	103.4	120	455	Carbon steel	2.04	2.03	1.00
Average												1.02
Cov												0.05

(b) Sections with fastened flanges

Specimen ID	Web	Flange	Lip	Bend radius	Thickness	Hole dia	Bearing length	Yield stress	Material	Exp.load	FEA result	P_{EXP}/P_{FEA}
	d	b_f	b_l	r	t	a	N	f_y		P_{EXP}	P_{FEA}	
	(mm)	(mm)	(mm)	(mm)	(mm)	(mm)	(mm)	(MPa)		(kN)	(kN)	
1	178.35	60.14	0	1.20	1.10	0	50	284	Stainless steel	2.33	2.27	1.02
2	178.57	60.13	0	1.20	1.12	68.94	50	284	Stainless steel	1.74	1.70	1.02

3	178.54	60.13	0	1.19	1.16	68.91	50	284	Stainless steel	2.34	2.38	0.98
4	178.56	60.06	0	1.20	1.15	0	75	284	Stainless steel	2.96	3.02	0.98
5	178.38	60.07	0	1.20	1.08	68.72	75	284	Stainless steel	1.91	1.88	1.02
6	178.56	60.07	0	1.20	1.12	68.74	75	284	Stainless steel	2.59	2.61	0.99
7	178.12	60.25	0	1.20	1.09	0	100	284	Stainless steel	3.02	3.08	0.98
8	178.64	60.04	0	1.20	1.07	68.88	100	284	Stainless steel	2.17	2.15	1.01
9	178.51	60.15	0	1.20	1.06	68.96	100	284	Stainless steel	2.64	2.64	1.00
10	203.55	74.97	0	1.19	1.16	0	50	284	Stainless steel	2.41	2.37	1.01
11	203.65	75.01	0	1.20	1.10	78.93	50	284	Stainless steel	1.50	1.43	1.05
12	203.62	75.04	0	1.20	1.15	78.94	50	284	Stainless steel	2.19	2.11	1.04
13	203.51	75.08	0	1.20	1.10	0	75	284	Stainless steel	2.45	2.42	1.01
14	203.59	75.01	0	1.20	1.11	78.91	75	284	Stainless steel	1.76	1.74	1.01
15	203.59	75.05	0	1.20	1.10	78.99	75	284	Stainless steel	2.22	2.22	1.00
16	203.56	75.04	0	1.20	1.09	0	100	284	Stainless steel	2.65	2.69	0.99
17	203.57	75.01	0	1.20	1.06	78.81	100	284	Stainless steel	1.82	1.81	1.00
18	203.62	74.97	0	1.20	1.05	78.82	100	284	Stainless steel	2.24	2.27	0.99
19	253.86	100.03	0	1.21	1.17	0	50	284	Stainless steel	2.09	2.03	1.03
20	253.88	99.99	0	1.20	1.39	98.81	50	284	Stainless steel	1.33	2.21	0.60
21	253.86	100.05	0	1.21	1.17	98.68	50	284	Stainless steel	1.91	1.85	1.03
22	253.57	99.96	0	1.19	1.16	0	75	284	Stainless steel	2.28	2.26	1.01
23	253.50	99.92	0	1.20	1.10	98.78	75	284	Stainless steel	1.39	1.34	1.03
24	253.48	100.02	0	1.20	1.13	98.83	75	284	Stainless steel	1.96	1.93	1.01
25	253.47	100.00	0	1.20	1.13	0	100	284	Stainless steel	2.34	2.38	0.98
26	253.44	99.98	0	1.20	1.08	98.87	100	284	Stainless steel	1.58	1.45	1.09
27	253.62	99.99	0	1.20	1.09	98.74	100	284	Stainless steel	2.03	1.98	1.02
Average												1.00
Cov												0.08

28	142.2	58.6	15.9	4.8	1.23	0	90	455	Carbon steel	3.75	3.97	0.94
29	172.8	64.1	15.6	5	1.27	0	90	455	Carbon steel	4.16	4.58	0.91
30	202.1	63.1	17.5	5	1.45	0	90	455	Carbon steel	5.24	5.62	0.93
31	202.1	63.1	17.5	5	1.45	0	90	455	Carbon steel	5.82	6.33	0.92
32	263.4	63.4	14.4	5.5	1.56	0	90	455	Carbon steel	5.06	5.08	1.00
33	263.4	63.4	14.4	5.5	1.56	0	120	455	Carbon steel	5.37	5.83	0.92
Average												0.94
Cov												0.03

Table 3 Web crippling coefficients for specimens without web holes under ITF and ETF cases

Support conditions	load cases	Coefficients [63-64]				Limitations			
		C	C_r	C_l	C_w	r_i/t_w	d_l/t_w	l_b/t_w	l_b/d_l
Flange fastened to support	ITF	20	0.10	0.08	0.031	≤ 12	≤ 200	≤ 210	≤ 2
	ETF	7.5	0.08	0.12	0.048	≤ 12			
Flange unfastened to support	ITF	24	0.52	0.15	0.001	≤ 1			
	ETF	13	0.32	0.05	0.04	≤ 1			

Table 4 Absolute percentage error collection for prediction of experimental results from Yousefi et al. [6-7]

(a) Sections with un-fastened flanges

Specimen ID	Web	Flange	Bend radius	Length	Thickness	Hole dia	Bearing length	Yield stress	Exp.load	Err (FEA)	Err (ASCE)	Err (EC)	Err (AISI&AS/NZS)	Err (DBN)	Err (BPN)	Err (Paddle)
	d	b_f	r	L	t	a	N	f_y	P_{EXP}							
	(mm)	(mm)	(mm)	(mm)	(mm)	(mm)	(mm)	(MPa)	(kN)							
1	178.54	60.1	1.2051	315.17	1.17	0	50	284	1.51	2.78	89.09	43.71	52.98	12.95	0.29	53.27
2-center hole	178.56	60.12	1.197	315	1.14	68.77	50	284	0.99	2.53	--	--	--	3.29	3.29	3.29
3-offset hole	178.29	60.2	1.1948	314.83	1.16	68.83	50	284	1.29	2.73	--	--	--	14.94	0.57	61.45
4	178.15	60.07	1.197	340	1.14	0	75	284	1.63	4.93	90.07	45.40	39.88	1.50	32.17	50.58
5-center hole	178.12	60.11	1.2036	339.67	1.18	68.76	75	284	1.25	2.87	--	--	--	2.39	42.39	66.39
6-offset hole	178.4	60.17	1.196	339.5	1.15	68.95	75	284	1.43	2.26	--	--	--	0.97	35.94	54.97
7	178.34	60.16	1.1978	364.67	1.13	0	100	284	1.76	3.92	95.25	49.43	32.39	9.12	26.17	47.69
8-center hole	178.46	60.04	1.196	364.17	1.15	68.86	100	284	1.33	5.10	--	--	--	15.72	0.68	59.47
9-offset hole	178.49	60.05	1.197	364.8	1.14	68.88	100	284	1.57	2.04	--	--	--	0.49	0.49	50.46
10	203.54	75.02	1.2051	349.67	1.17	0	50	284	1.39	6.72	89.66	45.32	55.40	0.26	0.26	0.26
11-center hole	203.58	74.96	1.2019	349.17	1.19	78.8	50	284	0.97	2.66	--	--	--	13.63	44.56	6.99
12-offset hole	203.57	74.98	1.1948	349	1.16	78.85	50	284	1.16	5.40	--	--	--	18.29	44.15	1.05
13	203.56	75	1.2051	374.67	1.17	0	75	284	1.44	0.52	110.46	61.11	57.64	8.61	43.34	8.61
14-center hole	203.37	74.98	1.2	374.67	1	78.81	75	284	0.99	33.26	--	--	--	4.07	24.27	105.08
15-offset hole	203.49	74.96	1.197	374.33	1.14	78.84	75	284	1.23	4.04	--	--	--	4.47	4.47	4.47
16	203.76	75.02	1.1984	399.33	1.12	0	100	284	1.51	6.18	104.41	53.64	37.09	11.86	34.50	51.59
17-center hole	203.64	74.94	1.1978	399.67	1.13	78.86	100	284	1.09	4.62	--	--	--	6.21	6.21	79.60
18-offset hole	203.68	75.01	1.1988	399.33	1.11	78.84	100	284	1.29	5.40	--	--	--	3.54	35.22	65.55
19	253.47	100.02	1.2019	424.33	1.19	0	50	284	1.14	3.23	102.46	54.39	72.81	6.17	50.03	64.01
20-center hole	253.52	100	1.2054	424.67	1.23	92.1	50	284	0.9	3.81	--	--	--	7.53	63.09	96.42

21-offset hole	253.54	99.98	1.2036	424.67	1.18	92.22	50	284	1.01	6.68	--	--	--	1.69	47.81	77.51
22	253.54	100	1.2	449.5	1.2	0	75	284	1.31	5.58	106.91	58.02	62.60	8.61	6.66	54.41
23-center hole	253.47	99.97	1.2	449.5	1.2	98.88	75	284	0.95	8.91	--	--	--	5.83	5.83	78.38
24-offset hole	254.57	99.99	1.196	448.67	1.15	98.75	75	284	1.02	7.29	--	--	--	5.43	43.59	5.43
25	253.59	100.02	1.2036	474.5	1.18	0	100	284	1.4	8.22	108.74	59.29	51.43	4.24	4.24	4.24
26-center hole	253.64	99.95	1.1988	474.5	1.08	98.8	100	284	0.97	27.28	--	--	--	5.70	14.92	14.92
27-offset hole	253.51	100	1.197	474.67	1.14	98.87	100	284	1.08	5.49	--	--	--	7.94	7.94	7.94
Average										6.46	99.67	52.26	51.36	6.87	23.08	43.48
Cov										7.06	8.20	6.18	12.20	4.86	19.61	31.76

(b) Sections with fastened flanges

Specimen ID	Web	Flange	Bend radius	Length	Thickness	Hole dia	Bearing length	Yield stress	Exp.load	Err (FEA)	Err (ASCE)	Err (EC)	Err (AISI&AS/NZS)	Err (DBN)	Err (BPN)	Err (Paddle)
	d	b_f	*r*	*L*	*t*	*a*	*N*	f_y	P_{EXP}							
	(mm)	(mm)	(mm)	(mm)	(mm)	(mm)	(mm)	(MPa)	(kN)							
1	178.35	60.14	1.20	314.83	1.10	0	50	284	2.33	2.38	5.69	19.31	27.90	9.01	9.01	17.60
2-center hole	178.57	60.13	1.20	314.83	1.12	68.94	50	284	1.74	2.23	--	--	--	12.79	12.79	1.30
3-offset hole	178.54	60.13	1.19	314.67	1.16	68.91	50	284	2.34	1.54	--	--	--	22.22	22.22	30.77
4	178.56	60.06	1.20	339.50	1.15	0	75	284	2.96	2.03	6.68	18.24	30.07	8.47	8.47	8.47
5-center hole	178.38	60.07	1.20	339.67	1.08	68.72	75	284	1.91	1.64	--	--	--	10.62	10.62	10.62
6-offset hole	178.56	60.07	1.20	339.67	1.12	68.74	75	284	2.59	0.74	--	--	--	23.74	27.60	31.47
7	178.12	60.25	1.20	364.50	1.09	0	100	284	3.02	1.89	4.89	19.87	35.76	10.05	15.02	11.71
8-center hole	178.64	60.04	1.20	365.00	1.07	68.88	100	284	2.17	0.85	--	--	--	5.00	11.92	7.31
9-offset hole	178.51	60.15	1.20	364.17	1.06	68.96	100	284	2.64	0.00	--	--	--	23.44	25.33	17.75
10	203.55	74.97	1.19	349.33	1.16	0	50	284	2.41	1.46	7.17	17.84	28.22	7.13	11.28	7.13
11-center hole	203.65	75.01	1.20	349.17	1.10	78.93	50	284	1.50	4.53	--	--	--	15.43	22.10	15.43

12-offset hole	203.62	75.04	1.20	349.33	1.15	78.94	50	284	2.19	3.44	--	--	--	24.48	24.48	33.61
13	203.51	75.08	1.20	374.50	1.10	0	75	284	2.45	1.35	6.34	18.78	32.65	7.22	3.14	7.22
14-center hole	203.59	75.01	1.20	374.33	1.11	78.91	75	284	1.76	1.25	--	--	--	17.49	11.81	17.49
15-offset hole	203.59	75.05	1.20	374.33	1.10	78.99	75	284	2.22	0.19	--	--	--	19.14	21.39	12.38
16	203.56	75.04	1.20	379.50	1.09	0	100	284	2.65	1.37	9.12	16.60	34.72	4.76	6.64	0.90
17-center hole	203.57	75.01	1.20	400.00	1.06	78.81	100	284	1.82	0.34	--	--	--	14.62	20.11	3.63
18-offset hole	203.62	74.97	1.20	399.00	1.05	78.82	100	284	2.24	1.19	--	--	--	21.04	21.04	21.04
19	253.86	100.03	1.21	424.83	1.17	0	50	284	2.09	2.95	5.04	20.10	32.06	7.45	5.06	5.06
20-offset hole	253.86	100.05	1.21	424.33	1.17	98.68	50	284	1.91	3.38	--	--	--	19.52	22.14	32.61
21	253.57	99.96	1.19	450.00	1.16	0	75	284	2.28	0.68	8.36	17.11	33.33	0.55	6.03	1.64
22-center hole	253.50	99.92	1.20	450.00	1.10	98.78	75	284	1.39	3.25	--	--	--	24.65	24.65	24.65
23-offset hole	253.48	100.02	1.20	449.67	1.13	98.83	75	284	1.96	1.48	--	--	--	18.67	18.67	28.88
24	253.47	100.00	1.20	474.50	1.13	0	100	284	2.34	1.60	11.14	15.38	35.47	0.26	0.26	8.28
25-center hole	253.44	99.98	1.20	474.50	1.08	98.87	100	284	1.58	8.05	--	--	--	17.59	11.26	17.59
26-offset hole	253.62	99.99	1.20	474.67	1.09	98.74	100	284	2.03	2.33	--	--	--	16.75	19.21	19.21
Average										2.01	7.16	18.14	32.24	13.93	15.09	15.14
Cov										1.61	1.94	1.48	2.79	7.32	7.58	15.05

Table 5 Statistical performance of the prediction models for F_{FEA}/F_p

Method	Training data			Validation data			Testing data		
	R^*	MSE	MAE	R^*	MSE	MAE	R^*	MSE	MAE
DBN	0.99	0.02	0.05	0.99	0.02	0.06	0.99	0.02	0.08
BPN	0.98	0.11	0.12	0.98	0.23	0.13	0.98	0.16	0.27
Paddle	0.95	0.22	0.42	0.97	0.23	0.43	0.95	0.28	0.46

Table 6 Average web crippling strength reduction factor (*R*) of investigated sections

Hole position \ Material		Ferritic		Duplex		Austenitic	
		Un-fastened flanges	Fastened flanges	Un-fastened flanges	Fastened flanges	Un-fastened flanges	Fastened flanges
Center hole	a/h=0.2	0.87	0.89	0.87	0.88	0.87	0.89
	a/h=0.4	0.71	0.77	0.71	0.75	0.72	0.77
	a/h=0.6	0.58	0.66	0.57	0.63	0.58	0.66
	a/h=0.8	0.45	0.51	0.46	0.50	0.46	0.51
Offset hole	a/h=0.2	0.95	0.97	0.96	0.97	0.95	0.97
	a/h=0.4	0.86	0.91	0.86	0.91	0.86	0.91
	a/h=0.6	0.76	0.84	0.76	0.85	0.76	0.83
	a/h=0.8	0.65	0.75	0.65	0.77	0.65	0.75

Table 7 Coefficients for cold-formed stainless steel channel section for end-two-flange loading case

Section type	Support and Flange conditions	Material	C		C_R	C_N	C_h	C_l
			C_1	C_2				
Lipped section	Unfastened to support	Ferritic stainless steel	6.834	5.126	0.258	0.215	0.046	0.004
		Duplex stainless steel	4.190	3.143	0.177	0.183	0.050	0.001
		Austenitic stainless steel	6.302	4.727	0.261	0.217	0.046	0.004
	Fastened to support	Ferritic stainless steel	7.320	5.124	0.237	0.306	0.038	0.022
		Duplex stainless steel	4.724	3.307	0.220	0.422	0.048	0.005
		Austenitic stainless steel	6.780	4.746	0.235	0.324	0.039	0.020
Unlipped section	Unfastened to support	Ferritic stainless steel	6.696	5.022	0.255	0.203	0.045	--
		Duplex stainless steel	3.981	2.986	0.169	0.171	0.050	--
		Austenitic stainless steel	6.157	4.618	0.257	0.206	0.045	--
	Fastened to support	Ferritic stainless steel	7.461	5.223	0.238	0.322	0.040	--
		Duplex stainless steel	4.257	2.980	0.223	0.463	0.049	--
		Austenitic stainless steel	6.964	4.875	0.237	0.335	0.041	--

Table 8 Comparison of proposed equations for web crippling strength with other calculation methods

(a) Sections with un-fastened flanges

Specimen ID	h/t	N/t	R/t	b_l/t	t (mm)	f_y (MPa)	$P_{Faliure}$ (kN)	$P_{Faliure}/P_{ASCE}$	$P_{Faliure}/P_{EC}$	$P_{Faliure}/P_{AISI\&AS/NZS}$	$P_{Faliure}/P_{prop}$
Unlipped cold-formed ferritic stainless steel [6-7]											
175x60-t1.2-N50-A0	149.54	42.74	1.03	0	1.17	284	1.51	0.53	0.70	0.65	1.00
175x60-t1.2-N75-A0	153.17	65.79	1.05	0	1.14	284	1.63	0.53	0.69	0.71	1.02
175x60-t1.2-N100-A0	154.70	88.50	1.06	0	1.13	284	1.76	0.51	0.67	0.76	1.02
200x75-t1.2-N50-A0	170.91	42.74	1.03	0	1.17	284	1.39	0.53	0.69	0.64	1.00
200x75-t1.2-N75-A0	170.92	64.10	1.03	0	1.17	284	1.44	0.48	0.62	0.63	0.92
200x75-t1.2-N100-A0	178.79	89.29	1.07	0	1.12	284	1.51	0.49	0.65	0.73	0.99
250x100-t1.2-N50-A0	209.98	42.02	1.01	0	1.19	284	1.14	0.49	0.65	0.58	0.94
250x100-t1.2-N75-A0	208.28	62.50	1.00	0	1.2	284	1.31	0.48	0.63	0.62	0.94
250x100-t1.2-N100-A0	211.87	84.75	1.02	0	1.18	284	1.40	0.48	0.63	0.66	0.96
Average								0.50	0.66	0.67	0.98
Cov								0.02	0.03	0.05	0.03
Lipped cold-formed ferritic stainless steel											
187×59×15-t1.5-N50-A0-FR	121.00	33.33	2.67	6.83	1.50	205.00	2.03	0.55	0.75	0.98	0.98
187×59×15-t1.5-N75-A0-FR	121.00	50.00	2.67	6.83	1.50	205.00	2.26	0.55	0.75	1.03	0.98
187×59×15-t1.5-N100-A0-FR	121.00	66.67	2.67	6.83	1.50	205.00	2.51	0.55	0.74	1.10	0.99
288×133×28-t1.5-N50-A0-FR	188.33	33.33	2.67	15.50	1.50	205.00	1.59	0.55	0.75	0.95	1.02
288×133×28-t1.5-N75-A0-FR	188.33	50.00	2.67	15.50	1.50	205.00	1.72	0.53	0.73	0.97	0.99
288×133×28-t1.5-N100-A0-FR	188.33	66.67	2.67	15.50	1.50	205.00	1.85	0.52	0.70	1.01	0.97
Average								0.54	0.74	1.01	0.99
Cov								0.01	0.02	0.05	0.02
Lipped cold-formed duplex stainless steel											
187×59×15-t1.5-N50-A0-FR	121.00	33.33	2.67	6.83	1.50	450.00	2.55	0.69	0.43	0.56	0.94
187×59×15-t1.5-N75-A0-FR	121.00	50.00	2.67	6.83	1.50	450.00	2.85	0.69	0.43	0.59	0.94
187×59×15-t1.5-N100-A0-FR	121.00	66.67	2.67	6.83	1.50	450.00	3.16	0.69	0.43	0.63	0.96
288×133×28-t1.5-N50-A0-FR	188.33	33.33	2.67	15.50	1.50	450.00	1.92	0.67	0.42	0.52	1.04
288×133×28-t1.5-N75-A0-FR	188.33	50.00	2.67	15.50	1.50	450.00	2.08	0.64	0.40	0.54	1.01

288×133×28-t1.5-N100-A0-FR	188.33	66.67	2.67	15.50	1.50	450.00	2.25	0.63	0.39	0.56	1.00
Average								0.67	0.42	0.57	0.98
Cov								0.03	0.02	0.04	0.04
Lipped cold-formed austenitic stainless steel											
187×59×15-t1.5-N50-A0-FR	121.00	33.33	2.67	6.83	1.50	205.00	1.88	0.51	0.70	0.90	0.99
187×59×15-t1.5-N75-A0-FR	121.00	50.00	2.67	6.83	1.50	205.00	2.09	0.51	0.69	0.96	0.98
187×59×15-t1.5-N100-A0-FR	121.00	66.67	2.67	6.83	1.50	205.00	2.32	0.50	0.69	1.02	0.99
288×133×28-t1.5-N50-A0-FR	188.33	33.33	2.67	15.50	1.50	205.00	1.48	0.51	0.70	0.88	1.04
288×133×28-t1.5-N75-A0-FR	188.33	50.00	2.67	15.50	1.50	205.00	1.60	0.49	0.68	0.91	1.00
288×133×28-t1.5-N100-A0-FR	188.33	66.67	2.67	15.50	1.50	205.00	1.72	0.48	0.65	0.94	0.98
Average								0.50	0.68	0.93	1.00
Cov								0.01	0.02	0.05	0.02

(b) Sections with fastened flanges

Specimen ID	h/t	N/t	R/t	b_l/t	t (mm)	f_y (MPa)	P_{Faliure} (kN)	$P_{\text{Faliure}}/P_{\text{ASCE}}$	$P_{\text{Faliure}}/P_{\text{EC}}$	$P_{\text{Faliure}}/P_{\text{AISI\&AS/NZS}}$	$P_{\text{Faliure}}/P_{\text{prop}}$
Unlipped cold-formed ferritic stainless steel [6-7]											
175x60-t1.2-N50-A0	158.96	45.45	1.09	0	1.10	284.00	2.33	0.95	1.24	1.39	1.10
175x60-t1.2-N75-A0	152.19	65.22	1.04	0	1.15	284.00	2.96	0.94	1.22	1.43	1.09
175x60-t1.2-N100-A0	160.21	91.74	1.10	0	1.09	284.00	3.02	0.95	1.25	1.56	1.13
200x75-t1.2-N50-A0	172.41	43.10	1.03	0	1.16	284.00	2.41	0.93	1.22	1.39	1.08
200x75-t1.2-N75-A0	181.83	68.18	1.09	0	1.10	284.00	2.45	0.94	1.23	1.48	1.08
200x75-t1.2-N100-A0	183.55	91.74	1.10	0	1.09	284.00	2.65	0.92	1.20	1.53	1.07
250x100-t1.2-N50-A0	213.91	42.74	1.03	0	1.17	284.00	2.09	0.95	1.25	1.47	1.05
250x100-t1.2-N75-A0	215.53	64.66	1.03	0	1.16	284.00	2.28	0.92	1.21	1.50	1.02
250x100-t1.2-N100-A0	221.19	88.50	1.06	0	1.13	284.00	2.34	0.90	1.18	1.55	1.00
Average								0.93	1.22	1.48	1.07
Cov								0.02	0.02	0.06	0.04
Lipped cold-formed ferritic stainless steel											
187×59×15-t1.5-N50-A0-FR	121.00	33.33	2.67	6.83	1.50	205.00	3.65	0.99	1.35	1.50	1.03
187×59×15-t1.5-N75-A0-FR	121.00	50.00	2.67	6.83	1.50	205.00	4.16	1.01	1.37	1.57	1.03
187×59×15-t1.5-N100-A0-FR	121.00	66.67	2.67	6.83	1.50	205.00	4.69	1.02	1.39	1.65	1.04

288×133×28-t1.5-N50-A0-FR	188.33	33.33	2.67	15.50	1.50	205.00	3.16	1.10	1.50	1.80	1.05
288×133×28-t1.5-N75-A0-FR	188.33	50.00	2.67	15.50	1.50	205.00	3.49	1.08	1.47	1.82	1.02
288×133×28-t1.5-N100-A0-FR	188.33	66.67	2.67	15.50	1.50	205.00	3.81	1.06	1.45	1.85	1.01
Average								1.04	1.42	1.70	1.03
Cov								0.04	0.05	0.13	0.02
Lipped cold-formed duplex stainless steel											
187×59×15-t1.5-N50-A0-FR	121.00	33.33	2.67	6.83	1.50	450.00	5.17	1.41	0.87	0.97	1.01
187×59×15-t1.5-N75-A0-FR	121.00	50.00	2.67	6.83	1.50	450.00	6.00	1.45	0.90	1.03	1.02
187×59×15-t1.5-N100-A0-FR	121.00	66.67	2.67	6.83	1.50	450.00	6.83	1.49	0.92	1.09	1.04
288×133×28-t1.5-N50-A0-FR	188.33	33.33	2.67	15.50	1.50	450.00	3.83	1.33	0.83	0.99	1.03
288×133×28-t1.5-N75-A0-FR	188.33	50.00	2.67	15.50	1.50	450.00	4.25	1.32	0.82	1.01	0.99
288×133×28-t1.5-N100-A0-FR	188.33	66.67	2.67	15.50	1.50	450.00	4.68	1.30	0.81	1.04	0.97
Average								1.38	0.86	1.02	1.01
Cov								0.07	0.04	0.04	0.02
Lipped cold-formed austenitic stainless steel											
187×59×15-t1.5-N50-A0-FR	121.00	33.33	2.67	6.83	1.50	205.00	3.45	0.94	1.28	1.42	1.03
187×59×15-t1.5-N75-A0-FR	121.00	50.00	2.67	6.83	1.50	205.00	3.95	0.96	1.30	1.49	1.03
187×59×15-t1.5-N100-A0-FR	121.00	66.67	2.67	6.83	1.50	205.00	4.46	0.97	1.32	1.57	1.05
288×133×28-t1.5-N50-A0-FR	188.33	33.33	2.67	15.50	1.50	205.00	3.00	1.04	1.43	1.70	1.07
288×133×28-t1.5-N75-A0-FR	188.33	50.00	2.67	15.50	1.50	205.00	3.31	1.02	1.40	1.72	1.03
288×133×28-t1.5-N100-A0-FR	188.33	66.67	2.67	15.50	1.50	205.00	3.61	1.00	1.37	1.75	1.02
Average								0.99	1.35	1.61	1.04
Cov								0.04	0.05	0.13	0.02

Notation: Specimen label follows the rules of Yousefi et al. [6-7]

Table 9 Proposed equations summary for web crippling strength reduction factor

Stainless steel grade		Lipped Channel section		Unlipped Channel section	
		Flange unfastened to support	Flange fastened to support	Flange unfastened to support	Flange fastened to support
Ferritic	α	0.966	0.985	0.967	0.969
	γ	0.689	0.636	0.694	0.611
	λ	0.095	0.139	0.090	0.107
	β	0.446	0.415	1.359	0.500
	μ	-0.785	-0.001	-0.727	-0.016
	ζ	-0.161	0.498	-0.099	0.420
	ξ	-0.544	0.765	-0.433	0.659
Duplex	α	0.961	0.974	0.960	0.966
	γ	0.684	0.650	0.687	0.630
	λ	0.103	0.138	0.101	0.101
	β	1.045	0.583	1.101	0.539
	μ	-0.525	-0.070	-0.554	-0.024
	ζ	0.084	0.358	0.058	0.388
	ξ	-0.018	0.557	-0.093	0.610
Austenitic	α	0.973	0.985	0.947	0.971
	γ	0.692	0.633	0.696	0.606
	λ	0.098	0.139	0.089	0.103
	β	1.588	0.406	1.468	0.500
	μ	-0.871	-0.001	-0.791	-0.019
	ζ	-0.254	0.507	-0.177	0.419
	ξ	-0.723	0.774	-0.570	0.659

Table 10 Comparison of proposed equations for web crippling strength reduction factor with other calculation methods

(a) For sections with un-fastened flanges

Specimen	Failure load without web holes	Reduction factor		Reduction factor		Reduction factor		Reduction factor		R/R_{Yousefi}		R/R_{Uzzaman}		R/R_{prop}	
	P_{A0}(kN)	$R=P_{\text{w}}/P_{\text{A0}}$		R_{Yousefi} by Yousefi [10-11, 15]		R by Uzzaman et al. [18-19]		R_{prop} by Equation							
		Center hole	Offset hole	Center hole	Offset hole	Center hole	Offset hole	Center hole	Offset hole	Center hole	Offset hole	Center hole	Offset hole	Center hole	Offset hole
Unlipped cold-formed ferritic stainless steel [6-7]															
175×60-t4.0-N50-A0.2-FR	28.20	0.84	0.98	0.84	1.01	0.82	--	0.85	0.95	1.01	0.96	1.03	--	0.98	1.03
175×60-t4.0-N50-A0.4-FR	28.20	0.67	0.89	0.68	0.91	0.70	--	0.72	0.85	0.98	0.98	0.96	--	0.93	1.04
175×60-t4.0-N50-A0.6-FR	28.20	0.52	0.79	0.53	0.80	0.58	--	0.58	0.75	0.98	0.98	0.91	--	0.91	1.05
200x75-t4.0-N75-A0.2-FR	30.93	0.83	0.94	0.84	0.99	0.83	--	0.86	0.98	0.98	0.95	1.00	--	0.96	0.96
200x75-t4.0-N75-A0.4-FR	30.93	0.66	0.88	0.69	0.88	0.71	--	0.72	0.88	0.95	0.99	0.93	--	0.91	1.00
200x75-t4.0-N75-A0.6-FR	30.93	0.53	0.81	0.54	0.78	0.59	--	0.59	0.77	0.99	1.05	0.91	--	0.91	1.05
250x100-t4.0-N100-A0.2-FR	30.93	0.82	0.94	0.84	0.99	0.83	--	0.87	0.97	0.98	0.95	0.99	--	0.95	0.97
250x100-t4.0-N100-A0.4-FR	30.93	0.67	0.90	0.69	0.89	0.71	--	0.73	0.87	0.96	1.02	0.94	--	0.92	1.04
250x100-t4.0-N100-A0.6-FR	30.93	0.54	0.79	0.54	0.78	0.59	--	0.59	0.77	0.99	1.01	0.91	--	0.91	1.03
Average										0.98	0.99	0.95		0.93	1.02
Cov										0.02	0.03	0.04		0.03	0.03
Lipped cold-formed ferritic stainless steel															
187×59×15-t1.5-N50-A0.2-FR	2.03	0.87	0.95	0.86	0.96	0.81	--	0.85	0.94	1.02	1.00	1.07	--	1.02	1.01
187×59×15-t1.5-N50-A0.4-FR	2.03	0.68	0.88	0.73	0.94	0.69	--	0.72	0.89	0.92	0.93	0.98	--	0.94	0.99
187×59×15-t1.5-N50-A0.6-FR	2.03	0.54	0.78	0.61	0.93	0.57	--	0.58	0.78	0.89	0.84	0.94	--	0.93	1.00
187×59×15-t1.5-N50-A0.8-FR	2.03	0.41	0.68	0.49	0.92	0.45	--	0.44	0.68	0.85	0.74	0.91	--	0.93	0.99

187×59×15-t1.5-N75-A0.2-FR	2.26	0.88	0.96	0.86	0.95	0.83	--	0.87	0.96	1.02	1.00	1.06	--	1.01	1.00
187×59×15-t1.5-N75-A0.4-FR	2.26	0.68	0.87	0.74	0.94	0.71	--	0.73	0.84	0.92	0.92	0.96	--	0.93	1.03
187×59×15-t1.5-N75-A0.6-FR	2.26	0.53	0.76	0.61	0.93	0.59	--	0.59	0.73	0.87	0.81	0.90	--	0.90	1.03
187×59×15-t1.5-N75-A0.8-FR	2.26	0.39	0.64	0.49	0.92	0.47	--	0.45	0.63	0.79	0.70	0.83	--	0.86	1.02
187×59×15-t1.5-N100-A0.2-FR	2.51	0.88	0.96	0.87	0.95	0.85	--	0.88	0.98	1.01	1.01	1.03	--	0.99	0.98
187×59×15-t1.5-N100-A0.4-FR	2.51	0.68	0.87	0.74	0.94	0.73	--	0.74	0.84	0.92	0.92	0.94	--	0.92	1.04
187×59×15-t1.5-N100-A0.6-FR	2.51	0.55	0.77	0.62	0.93	0.61	--	0.61	0.73	0.88	0.83	0.90	--	0.90	1.06
187×59×15-t1.5-N100-A0.8-FR	2.51	0.41	0.67	0.50	0.92	0.49	--	0.47	0.63	0.82	0.73	0.83	--	0.87	1.07
288×133×28-t1.5-N50-A0.2-FR	1.59	0.88	0.95	0.85	0.96	0.80	--	0.85	0.94	1.03	0.99	1.10	--	1.04	1.01
288×133×28-t1.5-N50-A0.4-FR	1.59	0.74	0.86	0.73	0.94	0.68	--	0.71	0.88	1.01	0.91	1.08	--	1.04	0.98
288×133×28-t1.5-N50-A0.6-FR	1.59	0.61	0.76	0.61	0.93	0.56	--	0.57	0.78	1.02	0.82	1.09	--	1.08	0.98
288×133×28-t1.5-N50-A0.8-FR	1.59	0.49	0.66	0.48	0.92	0.44	--	0.43	0.68	1.03	0.71	1.12	--	1.14	0.97
288×133×28-t1.5-N75-A0.2-FR	1.72	0.88	0.95	0.86	0.96	0.81	--	0.85	0.95	1.02	0.99	1.08	--	1.03	1.00
288×133×28-t1.5-N75-A0.4-FR	1.72	0.72	0.85	0.73	0.95	0.69	--	0.72	0.84	0.98	0.90	1.04	--	1.00	1.01
288×133×28-t1.5-N75-A0.6-FR	1.72	0.58	0.75	0.61	0.94	0.57	--	0.58	0.74	0.95	0.80	1.01	--	1.00	1.01
288×133×28-t1.5-N75-A0.8-FR	1.72	0.45	0.63	0.48	0.93	0.45	--	0.44	0.64	0.93	0.68	0.99	--	1.02	0.99
288×133×28-t1.5-N100-A0.2-FR	1.85	0.59	0.95	0.86	0.95	0.82	--	0.86	0.96	0.69	1.00	0.72	--	0.69	0.99
288×133×28-t1.5-N100-A0.4-FR	1.85	0.87	0.86	0.74	0.95	0.70	--	0.72	0.84	1.19	0.91	1.24	--	1.21	1.02
288×133×28-t1.5-N100-A0.6-FR	1.85	0.73	0.75	0.61	0.94	0.58	--	0.59	0.74	1.19	0.81	1.25	--	1.24	1.02
288×133×28-t1.5-N100-A0.8-FR	1.85	0.47	0.64	0.49	0.93	0.46	--	0.45	0.63	0.95	0.69	1.01	--	1.04	1.01
Average										0.95	0.86	1.00		0.99	1.01
Cov										0.11	0.11	0.12		0.11	0.02
Lipped cold-formed duplex stainless steel															
187×59×15-t1.5-N50-A0.2-FR	2.55	0.88	0.95	0.85	0.95	0.81	--	0.85	0.95	1.03	1.00	1.09	--	1.04	1.00
187×59×15-t1.5-N50-A0.4-FR	2.55	0.72	0.87	0.74	0.94	0.69	--	0.72	0.85	0.97	0.93	1.03	--	1.00	1.03
187×59×15-t1.5-N50-A0.6-FR	2.55	0.58	0.78	0.62	0.93	0.57	--	0.58	0.75	0.93	0.84	1.01	--	1.00	1.04
187×59×15-t1.5-N50-A0.8-FR	2.55	0.45	0.67	0.50	0.91	0.45	--	0.44	0.65	0.90	0.73	0.99	--	1.01	1.04
187×59×15-t1.5-N75-A0.2-FR	2.85	0.89	0.96	0.86	0.95	0.83	--	0.87	0.97	1.04	1.01	1.07	--	1.03	0.99

187×59×15-t1.5-N75-A0.4-FR	2.85	0.71	0.87	0.74	0.94	0.71	--	0.73	0.86	0.96	0.92	1.00	--	0.97	1.00
187×59×15-t1.5-N75-A0.6-FR	2.85	0.56	0.76	0.62	0.93	0.59	--	0.59	0.76	0.90	0.82	0.95	--	0.94	1.00
187×59×15-t1.5-N75-A0.8-FR	2.85	0.43	0.65	0.50	0.92	0.47	--	0.46	0.66	0.85	0.70	0.90	--	0.93	0.98
187×59×15-t1.5-N100-A0.2-FR	3.16	0.89	0.96	0.86	0.94	0.85	--	0.88	0.98	1.04	1.02	1.05	--	1.01	0.98
187×59×15-t1.5-N100-A0.4-FR	3.16	0.72	0.87	0.74	0.94	0.73	--	0.75	0.88	0.97	0.93	0.99	--	0.97	0.99
187×59×15-t1.5-N100-A0.6-FR	3.16	0.58	0.77	0.62	0.93	0.61	--	0.61	0.77	0.93	0.83	0.95	--	0.95	1.00
187×59×15-t1.5-N100-A0.8-FR	3.16	0.44	0.66	0.50	0.91	0.49	--	0.47	0.67	0.88	0.72	0.91	--	0.94	0.99
288×133×28-t1.5-N50-A0.2-FR	1.92	0.88	0.95	0.85	0.95	0.80	--	0.84	0.94	1.03	1.00	1.10	--	1.04	1.01
288×133×28-t1.5-N50-A0.4-FR	1.92	0.74	0.87	0.74	0.94	0.68	--	0.71	0.84	1.00	0.92	1.08	--	1.04	1.03
288×133×28-t1.5-N50-A0.6-FR	1.92	0.60	0.77	0.62	0.93	0.56	--	0.57	0.74	0.97	0.83	1.07	--	1.05	1.03
288×133×28-t1.5-N50-A0.8-FR	1.92	0.50	0.66	0.50	0.92	0.44	--	0.43	0.64	1.00	0.72	1.13	--	1.16	1.03
288×133×28-t1.5-N75-A0.2-FR	2.08	0.88	0.95	0.85	0.95	0.81	--	0.85	0.95	1.02	1.00	1.08	--	1.03	1.00
288×133×28-t1.5-N75-A0.4-FR	2.08	0.69	0.86	0.74	0.94	0.69	--	0.72	0.85	0.94	0.91	1.00	--	0.97	1.01
288×133×28-t1.5-N75-A0.6-FR	2.08	0.55	0.75	0.62	0.93	0.57	--	0.58	0.75	0.89	0.81	0.96	--	0.95	1.01
288×133×28-t1.5-N75-A0.8-FR	2.08	0.44	0.64	0.50	0.92	0.45	--	0.44	0.64	0.87	0.70	0.97	--	0.99	1.00
288×133×28-t1.5-N100-A0.2-FR	2.25	0.88	0.95	0.86	0.95	0.82	--	0.86	0.96	1.02	1.01	1.06	--	1.02	0.99
288×133×28-t1.5-N100-A0.4-FR	2.25	0.69	0.86	0.74	0.94	0.70	--	0.72	0.86	0.93	0.92	0.98	--	0.95	1.01
288×133×28-t1.5-N100-A0.6-FR	2.25	0.55	0.76	0.62	0.93	0.58	--	0.59	0.75	0.89	0.82	0.94	--	0.94	1.00
288×133×28-t1.5-N100-A0.8-FR	2.25	0.44	0.65	0.50	0.92	0.46	--	0.45	0.65	0.96	0.87	1.01		1.00	1.01
Average										0.06	0.11	0.06		0.05	0.02
Cov															
Lipped cold-formed austenitic stainless steel															
187×59×15-t1.5-N50-A0.2-FR	1.88	0.88	0.95	0.82	0.96	0.81	--	0.86	0.95	1.08	1.00	1.09	--	1.03	1.01
187×59×15-t1.5-N50-A0.4-FR	1.88	0.70	0.88	0.71	0.94	0.69	--	0.72	0.90	1.00	0.93	1.02	--	0.97	0.97
187×59×15-t1.5-N50-A0.6-FR	1.88	0.57	0.78	0.59	0.93	0.57	--	0.59	0.80	0.96	0.84	0.99	--	0.97	0.98
187×59×15-t1.5-N50-A0.8-FR	1.88	0.44	0.68	0.48	0.92	0.45	--	0.45	0.70	0.91	0.74	0.97	--	0.98	0.97
187×59×15-t1.5-N75-A0.2-FR	2.09	0.89	0.96	0.83	0.95	0.83	--	0.88	0.96	1.07	1.00	1.07	--	1.02	0.99
187×59×15-t1.5-N75-A0.4-FR	2.09	0.70	0.87	0.72	0.94	0.71	--	0.74	0.83	0.98	0.92	0.99	--	0.95	1.04

187×59×15-t1.5-N75-A0.6-FR	2.09	0.55	0.76	0.61	0.93	0.59	--	0.60	0.73	0.91	0.81	0.94	--	0.92	1.04
187×59×15-t1.5-N75-A0.8-FR	2.09	0.41	0.65	0.49	0.92	0.47	--	0.46	0.63	0.84	0.70	0.87	--	0.89	1.03
187×59×15-t1.5-N100-A0.2-FR	2.32	0.89	0.96	0.85	0.95	0.85	--	0.89	0.98	1.05	1.01	1.04	--	1.00	0.98
187×59×15-t1.5-N100-A0.4-FR	2.32	0.71	0.87	0.73	0.94	0.73	--	0.75	0.82	0.97	0.93	0.97	--	0.94	1.06
187×59×15-t1.5-N100-A0.6-FR	2.32	0.57	0.78	0.62	0.93	0.61	--	0.61	0.72	0.92	0.84	0.94	--	0.93	1.08
187×59×15-t1.5-N100-A0.8-FR	2.32	0.43	0.68	0.50	0.92	0.49	--	0.47	0.62	0.86	0.73	0.89	--	0.91	1.09
288×133×28-t1.5-N50-A0.2-FR	1.48	0.88	0.95	0.81	0.96	0.80	--	0.85	0.94	1.09	0.99	1.10	--	1.03	1.00
288×133×28-t1.5-N50-A0.4-FR	1.48	0.75	0.86	0.70	0.94	0.68	--	0.71	0.90	1.07	0.91	1.10	--	1.05	0.96
288×133×28-t1.5-N50-A0.6-FR	1.48	0.62	0.76	0.58	0.93	0.56	--	0.58	0.80	1.06	0.82	1.10	--	1.08	0.95
288×133×28-t1.5-N50-A0.8-FR	1.48	0.50	0.66	0.47	0.92	0.44	--	0.44	0.70	1.07	0.71	1.13	--	1.15	0.95
288×133×28-t1.5-N75-A0.2-FR	1.60	0.88	0.95	0.82	0.96	0.81	--	0.86	0.95	1.07	0.99	1.08	--	1.02	0.99
288×133×28-t1.5-N75-A0.4-FR	1.60	0.73	0.85	0.71	0.95	0.69	--	0.72	0.85	1.03	0.90	1.05	--	1.01	1.01
288×133×28-t1.5-N75-A0.6-FR	1.60	0.58	0.75	0.59	0.94	0.57	--	0.58	0.74	0.98	0.80	1.02	--	1.00	1.00
288×133×28-t1.5-N75-A0.8-FR	1.60	0.46	0.63	0.48	0.93	0.45	--	0.45	0.64	0.96	0.68	1.01	--	1.03	0.99
288×133×28-t1.5-N100-A0.2-FR	1.72	0.88	0.95	0.83	0.95	0.82	--	0.87	0.96	1.06	1.00	1.07	--	1.01	0.99
288×133×28-t1.5-N100-A0.4-FR	1.72	0.74	0.86	0.71	0.95	0.70	--	0.73	0.84	1.03	0.91	1.05	--	1.01	1.03
288×133×28-t1.5-N100-A0.6-FR	1.72	0.60	0.75	0.60	0.94	0.58	--	0.59	0.73	1.00	0.81	1.03	--	1.01	1.03
288×133×28-t1.5-N100-A0.8-FR	1.72	0.47	0.64	0.49	0.93	0.46	--	0.45	0.63	0.98	0.70	1.02	--	1.04	1.02
Average										1.00	0.86	1.02		1.00	1.01
Cov										0.07	0.11	0.07		0.06	0.04

(b) For sections with fastened flanges

Specimen	Failure load without web holes	Reduction factor		Reduction factor		Reduction factor		Reduction factor		$R/R_{Yousefi}$		$R/R_{Uzzaman}$		R/R_{prop}	
	P_{A0}(kN)	$R=P_w/P_{A0}$		$R_{Yousefi}$ by Yousefi [10-11, 15]		R by Uzzaman et al. [18-19]		R_{prop} by Equation							
		Center hole	Offset hole	Center hole	Offset hole	Center hole	Offset hole	Center hole	Offset hole	Center hole	Offset hole	Center hole	Offset hole	Center hole	Offset hole
Unlipped cold-formed ferritic stainless steel [6-7]															
175×60-t4.0-N50-A0.2-FR	28.20	0.84	0.98	0.84	1.01	0.82	--	0.88	0.98	1.01	0.96	1.03	--	0.96	1.00
175×60-t4.0-N50-A0.4-FR	28.20	0.67	0.89	0.68	0.91	0.70	--	0.72	0.91	0.98	0.98	0.96	--	0.93	0.98
175×60-t4.0-N50-A0.6-FR	28.20	0.52	0.79	0.53	0.80	0.58	--	0.58	0.84	0.98	0.98	0.91	--	0.91	0.94
200x75-t4.0-N75-A0.2-FR	30.93	0.83	0.94	0.84	0.99	0.83	--	0.86	0.96	0.98	0.95	1.00	--	0.96	0.98
200x75-t4.0-N75-A0.4-FR	30.93	0.66	0.88	0.69	0.88	0.71	--	0.72	0.89	0.95	0.99	0.93	--	0.91	0.99
200x75-t4.0-N75-A0.6-FR	30.93	0.53	0.81	0.54	0.78	0.59	--	0.59	0.82	0.99	1.05	0.91	--	0.91	0.99
250x100-t4.0-N100-A0.2-FR	30.93	0.82	0.94	0.84	0.99	0.83	--	0.87	0.97	0.98	0.95	0.99	--	0.95	0.97
250x100-t4.0-N100-A0.4-FR	30.93	0.67	0.90	0.69	0.89	0.71	--	0.73	0.91	0.96	1.02	0.94	--	0.92	1.00
250x100-t4.0-N100-A0.6-FR	30.93	0.54	0.79	0.54	0.78	0.59	--	0.59	0.84	0.99	1.01	0.91	--	0.91	0.94
Average										0.98	0.99	0.95		0.93	0.98
Cov										0.02	0.03	0.04		0.02	0.02
Lipped cold-formed ferritic stainless steel															
187×59×15-t1.5-N50-A0.2-FR	3.65	0.91	0.98	0.91	0.98	0.81	--	0.90	0.98	0.99	0.99	1.11	--	1.01	1.00
187×59×15-t1.5-N50-A0.4-FR	3.65	0.76	0.90	0.77	0.94	0.69	--	0.77	0.84	0.99	0.95	1.10	--	0.99	1.07
187×59×15-t1.5-N50-A0.6-FR	3.65	0.66	0.79	0.62	0.90	0.57	--	0.64	0.76	1.06	0.88	1.15	--	1.02	1.04
187×59×15-t1.5-N50-A0.8-FR	3.65	0.48	0.74	0.48	0.86	0.45	--	0.52	0.68	1.01	0.85	1.06	--	0.93	1.08
187×59×15-t1.5-N75-A0.2-FR	4.16	0.91	0.98	0.92	0.98	0.83	--	0.92	0.99	0.98	1.00	1.09	--	0.99	0.99
187×59×15-t1.5-N75-A0.4-FR	4.16	0.75	0.88	0.78	0.94	0.71	--	0.79	0.94	0.96	0.94	1.05	--	0.95	0.94
187×59×15-t1.5-N75-A0.6-FR	4.16	0.64	0.79	0.63	0.90	0.59	--	0.66	0.87	1.01	0.87	1.08	--	0.97	0.91

187×59×15-t1.5-N75-A0.8-FR	4.16	0.41	0.73	0.49	0.86	0.47	--	0.53	0.79	0.84	0.84	0.87	--	0.76	0.92
187×59×15-t1.5-N100-A0.2-FR	4.69	0.90	0.98	0.93	0.98	0.85	--	0.94	1.01	0.96	1.00	1.06	--	0.96	0.97
187×59×15-t1.5-N100-A0.4-FR	4.69	0.77	0.89	0.79	0.94	0.73	--	0.81	0.99	0.98	0.95	1.06	--	0.95	0.91
187×59×15-t1.5-N100-A0.6-FR	4.69	0.67	0.79	0.64	0.90	0.61	--	0.68	0.91	1.04	0.87	1.10	--	0.98	0.86
187×59×15-t1.5-N100-A0.8-FR	4.69	0.45	0.69	0.50	0.86	0.49	--	0.55	0.83	0.91	0.80	0.93	--	0.82	0.83
288×133×28-t1.5-N50-A0.2-FR	3.16	0.92	0.96	0.91	0.99	0.80	--	0.88	0.95	1.01	0.97	1.14	--	1.04	1.01
288×133×28-t1.5-N50-A0.4-FR	3.16	0.84	0.92	0.76	0.94	0.68	--	0.76	0.81	1.10	0.98	1.23	--	1.11	1.13
288×133×28-t1.5-N50-A0.6-FR	3.16	0.75	0.84	0.61	0.90	0.56	--	0.63	0.74	1.23	0.94	1.34	--	1.20	1.15
288×133×28-t1.5-N50-A0.8-FR	3.16	0.60	0.77	0.47	0.86	0.44	--	0.50	0.66	1.29	0.89	1.37	--	1.20	1.16
288×133×28-t1.5-N75-A0.2-FR	3.49	0.91	0.96	0.91	0.98	0.81	--	0.90	0.96	1.00	0.98	1.12	--	1.02	1.00
288×133×28-t1.5-N75-A0.4-FR	3.49	0.83	0.90	0.77	0.94	0.69	--	0.77	0.89	1.08	0.95	1.19	--	1.08	1.01
288×133×28-t1.5-N75-A0.6-FR	3.49	0.72	0.82	0.62	0.91	0.57	--	0.64	0.82	1.16	0.91	1.26	--	1.13	1.01
288×133×28-t1.5-N75-A0.8-FR	3.49	0.54	0.72	0.47	0.87	0.45	--	0.51	0.74	1.14	0.83	1.19	--	1.05	0.97
288×133×28-t1.5-N100-A0.2-FR	3.81	0.90	0.97	0.92	0.98	0.82	--	0.91	0.97	0.98	0.99	1.10	--	1.00	1.00
288×133×28-t1.5-N100-A0.4-FR	3.81	0.84	0.91	0.77	0.94	0.70	--	0.78	0.92	1.08	0.96	1.19	--	1.07	0.98
288×133×28-t1.5-N100-A0.6-FR	3.81	0.75	0.83	0.63	0.90	0.58	--	0.65	0.85	1.19	0.91	1.28	--	1.14	0.97
288×133×28-t1.5-N100-A0.8-FR	3.81	0.57	0.74	0.48	0.87	0.46	--	0.53	0.77	1.18	0.85	1.23	--	1.08	0.95
Average										1.05	0.92	1.14		1.02	0.99
Cov										0.10	0.06	0.11		0.10	0.08
Lipped cold-formed duplex stainless steel															
187×59×15-t1.5-N50-A0.2-FR	5.17	0.91	0.97	0.89	0.98	0.81	--	0.88	0.98	1.01	0.99	1.11	--	1.03	1.00
187×59×15-t1.5-N50-A0.4-FR	5.17	0.73	0.92	0.74	0.98	0.69	--	0.75	0.86	0.99	0.94	1.06	--	0.97	1.07
187×59×15-t1.5-N50-A0.6-FR	5.17	0.61	0.84	0.59	0.97	0.57	--	0.62	0.79	1.04	0.87	1.07	--	0.98	1.07
187×59×15-t1.5-N50-A0.8-FR	5.17	0.48	0.74	0.44	0.97	0.45	--	0.49	0.72	1.09	0.77	1.05	--	0.97	1.03
187×59×15-t1.5-N75-A0.2-FR	6.00	0.91	0.98	0.91	0.98	0.83	--	0.90	0.99	1.00	1.00	1.09	--	1.01	0.99
187×59×15-t1.5-N75-A0.4-FR	6.00	0.72	0.91	0.75	0.98	0.71	--	0.77	0.94	0.96	0.93	1.02	--	0.94	0.97
187×59×15-t1.5-N75-A0.6-FR	6.00	0.59	0.83	0.60	0.97	0.59	--	0.64	0.87	0.98	0.85	1.00	--	0.92	0.96
187×59×15-t1.5-N75-A0.8-FR	6.00	0.43	0.73	0.45	0.97	0.47	--	0.51	0.80	0.96	0.75	0.92	--	0.85	0.91

187×59×15-t1.5-N100-A0.2-FR	6.83	0.90	0.98	0.92	0.98	0.85	--	0.92	1.00	0.98	1.00	1.06	--	0.98	0.98
187×59×15-t1.5-N100-A0.4-FR	6.83	0.73	0.91	0.77	0.98	0.73	--	0.79	0.97	0.95	0.93	1.00	--	0.92	0.94
187×59×15-t1.5-N100-A0.6-FR	6.83	0.60	0.83	0.61	0.97	0.61	--	0.66	0.90	0.98	0.86	1.00	--	0.91	0.92
187×59×15-t1.5-N100-A0.8-FR	6.83	0.46	0.72	0.46	0.97	0.49	--	0.53	0.83	1.00	0.75	0.95	--	0.87	0.87
288×133×28-t1.5-N50-A0.2-FR	3.83	0.89	0.97	0.88	0.98	0.80	--	0.87	0.96	1.01	0.98	1.11	--	1.03	1.01
288×133×28-t1.5-N50-A0.4-FR	3.83	0.83	0.92	0.73	0.98	0.68	--	0.74	0.84	1.13	0.94	1.21	--	1.12	1.09
288×133×28-t1.5-N50-A0.6-FR	3.83	0.73	0.86	0.58	0.97	0.56	--	0.61	0.77	1.26	0.88	1.30	--	1.20	1.11
288×133×28-t1.5-N50-A0.8-FR	3.83	0.60	0.78	0.43	0.97	0.44	--	0.48	0.70	1.39	0.81	1.35	--	1.24	1.10
288×133×28-t1.5-N75-A0.2-FR	4.25	0.89	0.97	0.89	0.98	0.81	--	0.88	0.97	1.00	0.99	1.10	--	1.01	1.00
288×133×28-t1.5-N75-A0.4-FR	4.25	0.78	0.91	0.74	0.98	0.69	--	0.75	0.90	1.05	0.93	1.13	--	1.04	1.01
288×133×28-t1.5-N75-A0.6-FR	4.25	0.65	0.84	0.59	0.97	0.57	--	0.62	0.83	1.11	0.87	1.14	--	1.05	1.01
288×133×28-t1.5-N75-A0.8-FR	4.25	0.50	0.75	0.44	0.97	0.45	--	0.49	0.76	1.15	0.78	1.11	--	1.02	0.99
288×133×28-t1.5-N100-A0.2-FR	4.68	0.89	0.97	0.90	0.98	0.82	--	0.89	0.97	0.99	0.99	1.08	--	1.00	1.00
288×133×28-t1.5-N100-A0.4-FR	4.68	0.80	0.92	0.75	0.98	0.70	--	0.76	0.92	1.08	0.94	1.14	--	1.05	0.99
288×133×28-t1.5-N100-A0.6-FR	4.68	0.68	0.85	0.60	0.97	0.58	--	0.63	0.85	1.14	0.88	1.17	--	1.08	0.99
288×133×28-t1.5-N100-A0.8-FR	4.68	0.53	0.76	0.44	0.97	0.46	--	0.50	0.78	1.20	0.79	1.15	--	1.06	0.97
Average										1.06	0.89	1.10		1.01	1.00
Cov										0.11	0.08	0.10		0.09	0.06
Lipped cold-formed austenitic stainless steel															
187×59×15-t1.5-N50-A0.2-FR	3.45	0.91	0.98	0.87	0.87	0.81	--	0.90	0.97	1.05	1.12	1.12	--	1.02	1.00
187×59×15-t1.5-N50-A0.4-FR	3.45	0.76	0.90	0.74	0.70	0.69	--	0.77	0.83	1.02	1.29	1.09	--	0.98	1.08
187×59×15-t1.5-N50-A0.6-FR	3.45	0.64	0.80	0.61	0.52	0.57	--	0.64	0.75	1.05	1.54	1.12	--	1.00	1.06
187×59×15-t1.5-N50-A0.8-FR	3.45	0.49	0.73	0.48	0.35	0.45	--	0.52	0.68	1.01	2.09	1.08	--	0.95	1.08
187×59×15-t1.5-N75-A0.2-FR	3.95	0.91	0.98	0.88	0.87	0.83	--	0.92	0.99	1.04	1.12	1.10	--	0.99	0.99
187×59×15-t1.5-N75-A0.4-FR	3.95	0.75	0.88	0.75	0.70	0.71	--	0.79	0.94	1.00	1.26	1.06	--	0.95	0.93
187×59×15-t1.5-N75-A0.6-FR	3.95	0.63	0.79	0.62	0.53	0.59	--	0.66	0.87	1.02	1.51	1.07	--	0.95	0.92
187×59×15-t1.5-N75-A0.8-FR	3.95	0.44	0.73	0.49	0.35	0.47	--	0.54	0.79	0.89	2.07	0.93	--	0.82	0.92
187×59×15-t1.5-N100-A0.2-FR	4.46	0.90	0.98	0.89	0.87	0.85	--	0.94	1.01	1.02	1.13	1.06	--	0.96	0.97

187×59×15-t1.5-N100-A0.4-FR	4.46	0.76	0.90	0.76	0.70	0.73	--	0.81	0.98	1.00	1.29	1.05	--	0.94	0.91
187×59×15-t1.5-N100-A0.6-FR	4.46	0.64	0.79	0.63	0.52	0.61	--	0.68	0.91	1.02	1.51	1.06	--	0.94	0.87
187×59×15-t1.5-N100-A0.8-FR	4.46	0.48	0.69	0.50	0.35	0.49	--	0.56	0.83	0.95	1.97	0.98	--	0.85	0.83
288×133×28-t1.5-N50-A0.2-FR	3.00	0.91	0.96	0.86	0.88	0.80	--	0.88	0.95	1.06	1.09	1.14	--	1.03	1.01
288×133×28-t1.5-N50-A0.4-FR	3.00	0.85	0.92	0.73	0.70	0.68	--	0.76	0.81	1.15	1.32	1.24	--	1.12	1.14
288×133×28-t1.5-N50-A0.6-FR	3.00	0.77	0.84	0.61	0.52	0.56	--	0.63	0.73	1.27	1.61	1.37	--	1.22	1.15
288×133×28-t1.5-N50-A0.8-FR	3.00	0.64	0.77	0.48	0.35	0.44	--	0.50	0.65	1.33	2.19	1.45	--	1.27	1.17
288×133×28-t1.5-N75-A0.2-FR	3.31	0.91	0.96	0.87	0.87	0.81	--	0.90	0.96	1.05	1.10	1.12	--	1.01	1.00
288×133×28-t1.5-N75-A0.4-FR	3.31	0.82	0.90	0.74	0.70	0.69	--	0.77	0.89	1.11	1.28	1.18	--	1.06	1.01
288×133×28-t1.5-N75-A0.6-FR	3.31	0.70	0.82	0.61	0.53	0.57	--	0.64	0.81	1.14	1.56	1.22	--	1.08	1.01
288×133×28-t1.5-N75-A0.8-FR	3.31	0.53	0.71	0.48	0.35	0.45	--	0.52	0.74	1.10	2.02	1.18	--	1.04	0.97
288×133×28-t1.5-N100-A0.2-FR	3.61	0.90	0.97	0.87	0.87	0.82	--	0.91	0.97	1.03	1.11	1.10	--	0.99	0.99
288×133×28-t1.5-N100-A0.4-FR	3.61	0.83	0.91	0.75	0.70	0.70	--	0.78	0.92	1.12	1.30	1.19	--	1.07	0.99
288×133×28-t1.5-N100-A0.6-FR	3.61	0.73	0.83	0.62	0.53	0.58	--	0.66	0.85	1.18	1.57	1.25	--	1.12	0.98
288×133×28-t1.5-N100-A0.8-FR	3.61	0.57	0.74	0.49	0.35	0.46	--	0.53	0.77	1.17	2.09	1.24	--	1.09	0.96
Average										1.07	1.51	1.14		1.02	1.00
Cov										0.10	0.36	0.11		0.10	0.08

Notation: Specimen label follows the rules of Yousefi et al. [6-7]

Table 11 Comparison of DBN output data with the proposed web crippling strength of cold-formed stainless steel channel section

(a) With un-fastened flanges

	Ferritic stainless steel	Duplex stainless steel	Austenitic stainless steel
Ratio of equations	P_{DBN} / P_{prop}	P_{DBN} / P_{prop}	P_{DBN} / P_{prop}
Data number	247	255	249
Mean, P_m	1.02	1.02	1.02
Coefficient of variation, COV	0.07	0.07	0.07
Reliability index, β [2,63]	2.76	2.78	2.77
Resistance factor, φ [2,63]	0.85	0.85	0.85
Reliability index, β [28]	3.30	3.33	3.31
Resistance factor, φ [28]	0.70	0.70	0.70

(b) With fastened flanges

	Ferritic stainless steel	Duplex stainless steel	Austenitic stainless steel
Ratio of equations	P_{DBN} / P_{prop}	P_{DBN} / P_{prop}	P_{DBN} / P_{prop}
Data number	288	260	279
Mean, P_m	1.02	1.02	1.02
Coefficient of variation, COV	0.08	0.07	0.07
Reliability index, β [2,63]	2.77	2.78	2.76
Resistance factor, φ [2,63]	0.85	0.85	0.85
Reliability index, β [28]	3.31	3.33	3.30
Resistance factor, φ [28]	0.70	0.70	0.70

Table 12 Comparison of DBN output data with the proposed web crippling strength reduction factor of cold-formed stainless steel channel section

(a) With un-fastened flanges and centered web hole

	Ferritic stainless steel	Duplex stainless steel	Austenitic stainless steel
Ratio of equations	R_{DBN} / R_{prop}	R_{DBN} / R_{prop}	R_{DBN} / R_{prop}
Data number	1440	1439	1441
Mean, P_m	1.00	1.00	1.00
Coefficient of variation, COV	0.04	0.04	0.04
Reliability index, β [2,63]	2.70	2.70	2.70
Resistance factor, φ [2,63]	0.85	0.85	0.85
Reliability index, β [28]	3.24	3.24	
Resistance factor, φ [28]	0.70	0.70	0.70

(b) With un-fastened flanges and offset web hole

	Ferritic stainless steel	Duplex stainless steel	Austenitic stainless steel
Ratio of equations	R_{DBN} / R_{prop}	R_{DBN} / R_{prop}	R_{DBN} / R_{prop}
Data number	1425	1430	1426
Mean, P_m	1.00	1.00	1.00
Coefficient of variation, COV	0.04	0.03	0.04
Reliability index, β [2,63]	2.70	2.70	2.70
Resistance factor, φ [2,63]	0.85	0.85	0.85
Reliability index, β [28]	3.24	3.24	3.24
Resistance factor, φ [28]	0.70	0.70	0.70

(c) With fastened flanges and centered web hole

	Ferritic stainless steel	Duplex stainless steel	Austenitic stainless steel
Ratio of equations	R_{DBN} / R_{prop}	R_{DBN} / R_{prop}	R_{DBN} / R_{prop}
Data number	1440	1441	1439
Mean, P_m	1.00	1.00	1.00
Coefficient of variation, COV	0.07	0.06	0.07
Reliability index, β [2,63]	2.69	2.70	2.69
Resistance factor, φ [2,63]	0.85	0.85	0.85
Reliability index, β [28]	3.24	3.24	3.24
Resistance factor, φ [28]	0.70	0.70	0.70

(d) With fastened flanges and offset web hole

	Ferritic stainless steel	Duplex stainless steel	Austenitic stainless steel
Ratio of equations	R_{DBN} / R_{prop}	R_{DBN} / R_{prop}	R_{DBN} / R_{prop}
Data number	1419	1417	1417
Mean, P_m	1.00	1.00	1.00
Coefficient of variation, COV	0.03	0.02	0.03
Reliability index, β [2,63]	2.70	2.70	2.70
Resistance factor, φ [2,63]	0.85	0.85	0.85
Reliability index, β [28]	3.24	3.24	3.24
Resistance factor, φ [28]	0.70	0.70	0.70

List of figures

Fig.9 Web crippling strength against b_l/t

(a) Comparison of lipped and unlipped sections with un-fastened flanges

(b) Comparison of lipped and unlipped sections with fastened flanges

(c) Web crippling strength of sections with fastened flanges against b_l/t

Fig.10 Web crippling strength reduction factor against *a/h*

(a) Cold-formed ferritic stainless steel channel section with center web hole

(b) Cold-formed duplex stainless steel channel section with center web hole

(c) Cold-formed austenitic stainless steel channel section with center web hole

(d) Cold-formed ferritic stainless steel channel section with offset web hole

(e) Cold-formed duplex stainless steel channel section with offset web hole

(f) Cold-formed austenitic stainless steel channel section with offset web hole

Fig.11 Web crippling strength reduction factor against *x/h*

(a) Sections with un-fastened flanges in Ferritic stainless steel

(b) Sections with fastened flanges in Ferritic stainless steel

(c) Sections with un-fastened flanges in Duplex stainless steel

(d) Sections with fastened flanges in Duplex stainless steel

(e) Sections with un-fastened flanges in Austenitic stainless steel

(f) Sections with fastened flanges in Austenitic stainless steel

Fig.12 Web crippling strength reduction factor against *N/h*

(a) Sections with un-fastened flanges in Ferritic stainless steel with center web hole

(b) Sections with fastened flanges in Ferritic stainless steel with center web hole

(c) Sections with un-fastened flanges in Duplex stainless steel with center web hole

(d) Sections with fastened flanges in Duplex stainless steel with center web hole

(e) Sections with un-fastened flanges in Austenitic stainless steel with center web hole

(f) Sections with fastened flanges in Austenitic stainless steel with center web hole

(g) Sections with un-fastened flanges in Ferritic stainless steel with offset web hole

(h) Sections with fastened flanges in Ferritic stainless steel with offset web hole

(i) Sections with un-fastened flanges in Duplex stainless steel with offset web hole

(j) Sections with fastened flanges in Duplex stainless steel with offset web hole

(k) Sections with un-fastened flanges in Austenitic stainless steel with offset web hole

(l) Sections with fastened flanges in Austenitic stainless steel with offset web hole

Fig.13 Web crippling strength reduction factor against un-fastened/fastened flanges

(a) Cold-formed ferritic stainless steel channel section with center web hole

(b) Cold-formed duplex stainless steel channel section with center web hole

(c) Cold-formed austenitic stainless steel channel section with center web hole

(d) Cold-formed ferritic stainless steel channel section with offset web hole

(e) Cold-formed duplex stainless steel channel section with offset web hole

(f) Cold-formed austenitic stainless steel channel section with offset web hole

(a) Structural stainless steel at Gent Sint Pieters railway station in Belgium. Photo: Patrick Lints [1]

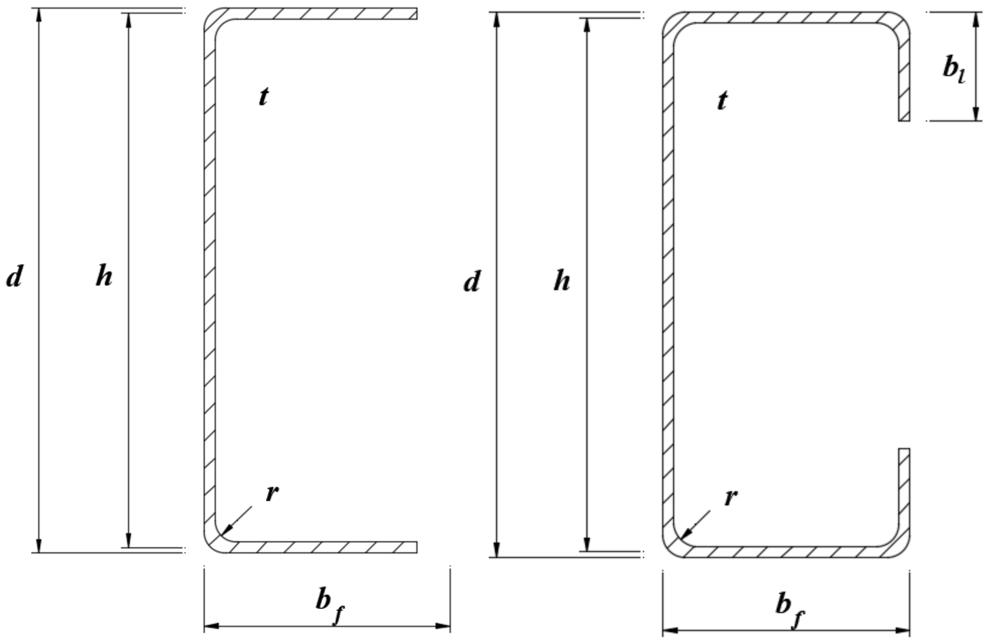

(b) Definition of symbols

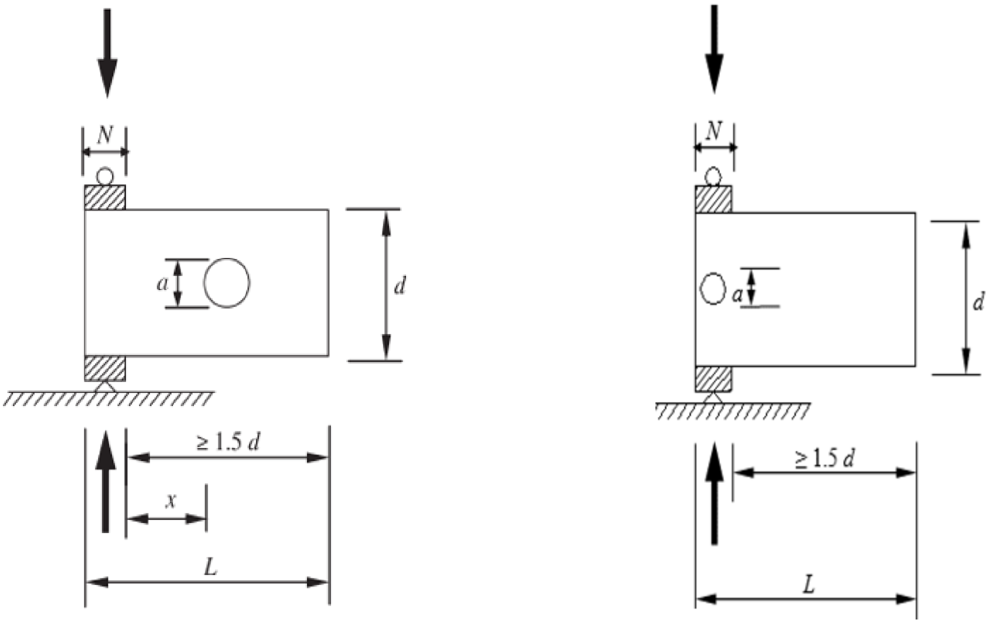

(c) ETF loading condition with offset web hole

(d) ETF loading condition center web hole

Fig.1 Introduction to web crippling

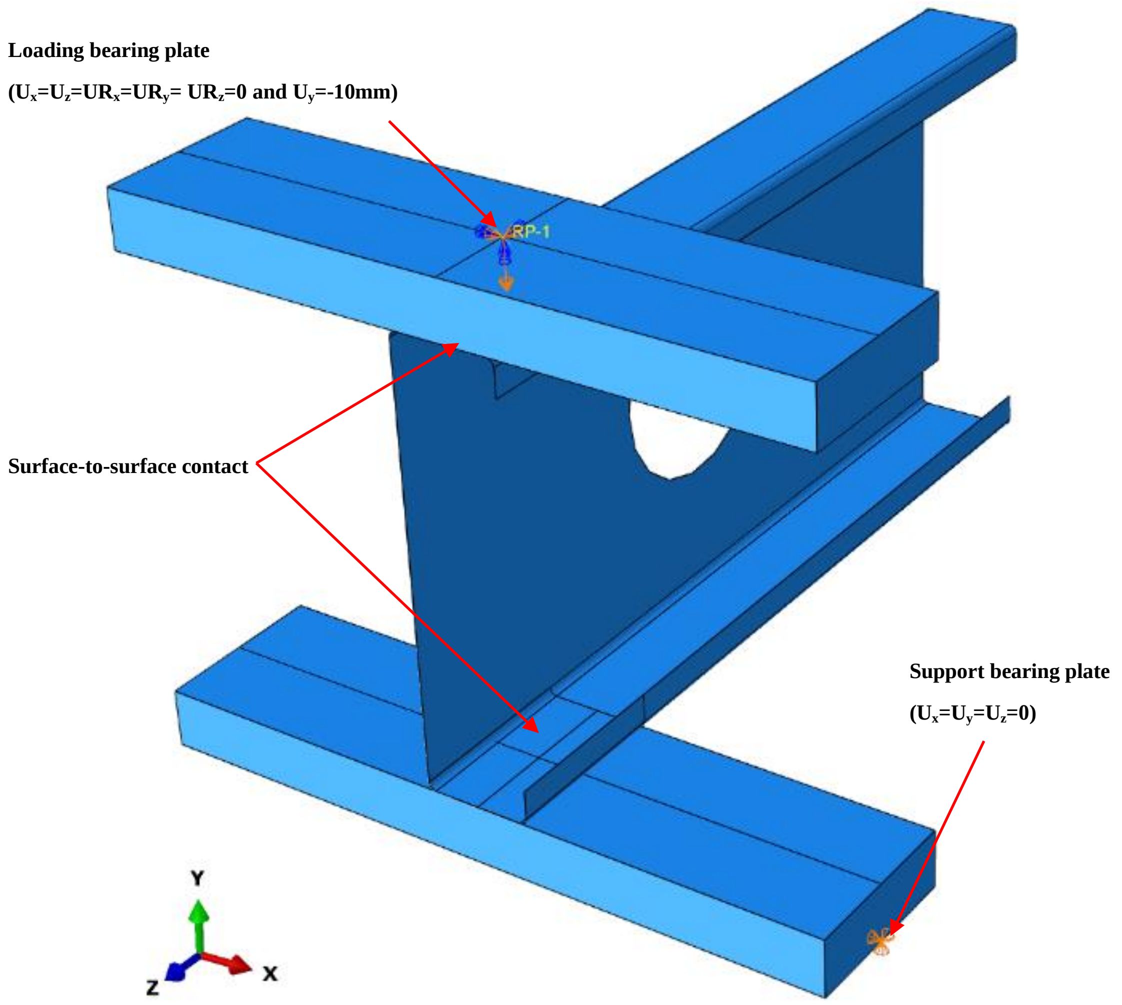

Fig.2 Boundary conditions used in the FE models

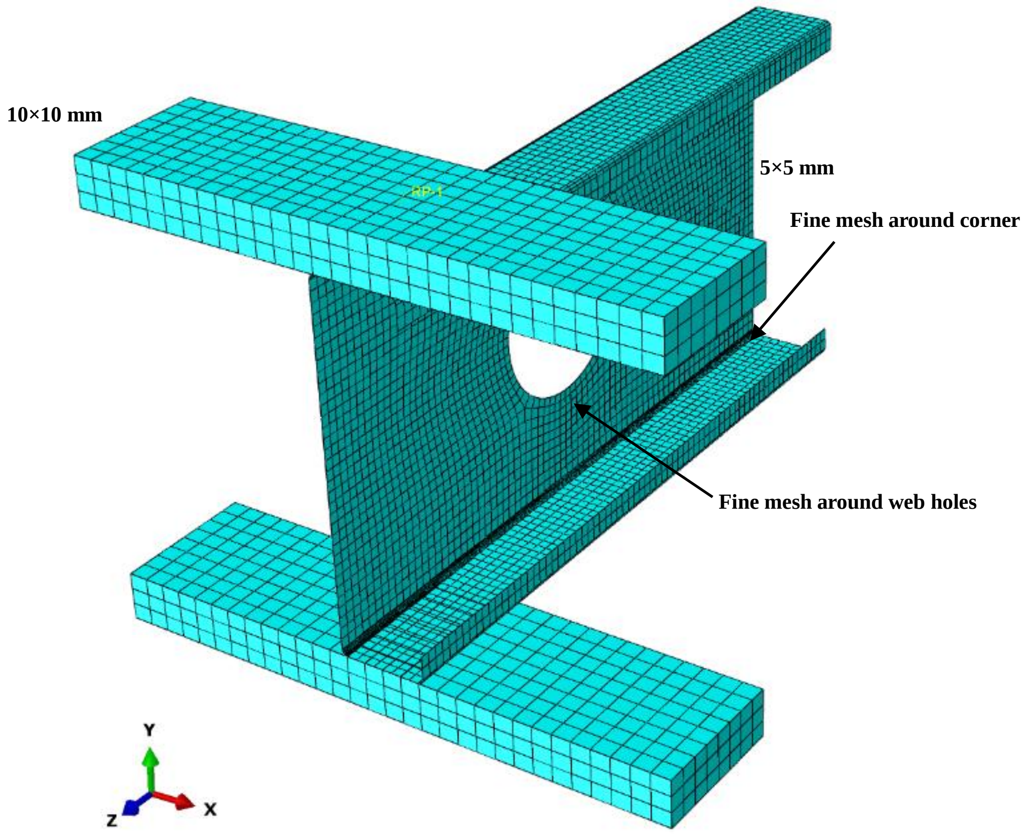

Fig.3 FE meshing types

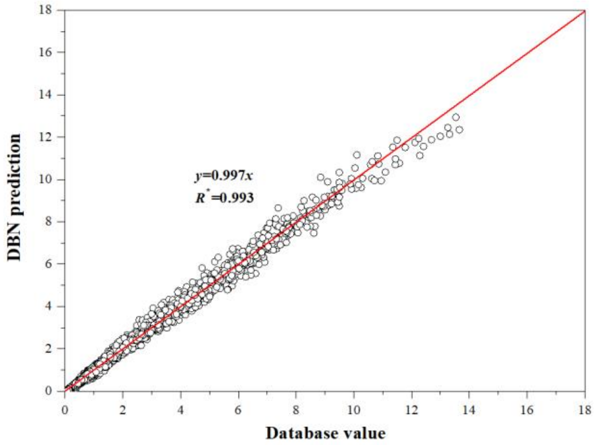

(a) Training set

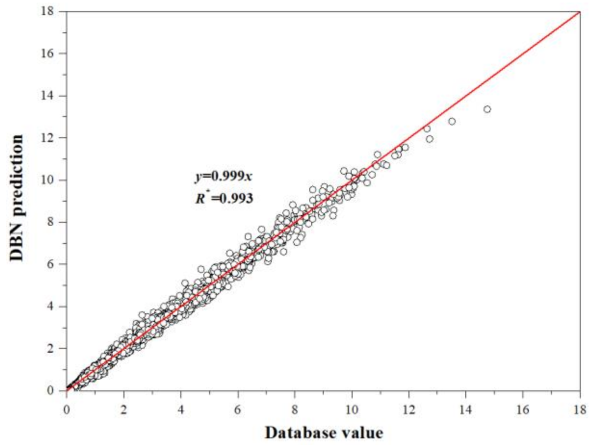

(b) Validation set

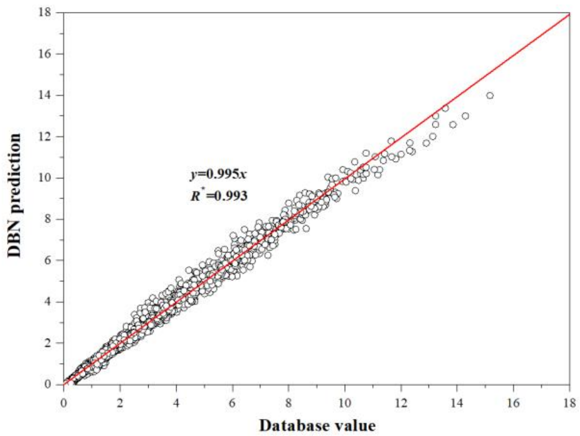

(c) Testing set

Fig.4 Predicted results using DBN

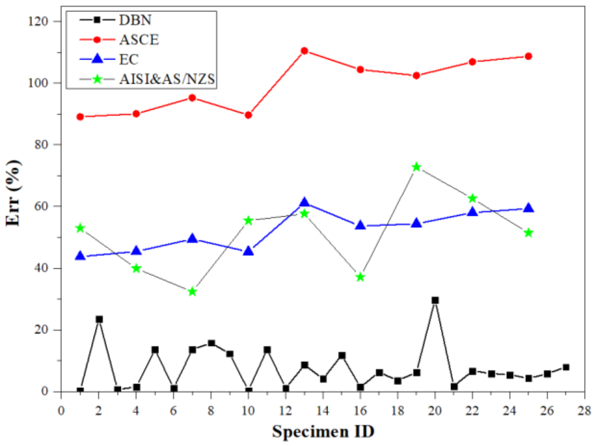

(a) DBN, ASCE, EC and AISI&AS/NZS for sections with un-fastened flanges

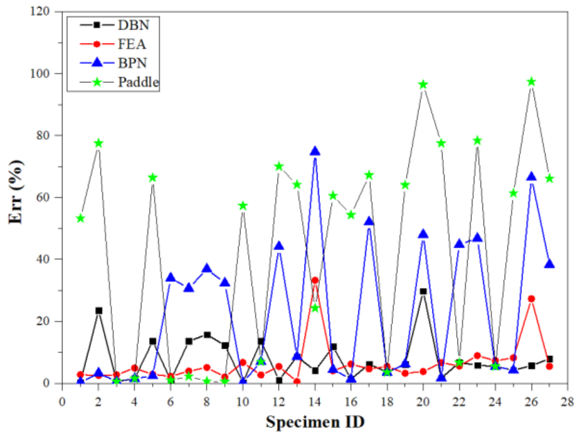

(b) DBN, FEA, BPN and Paddle for sections with un-fastened flanges

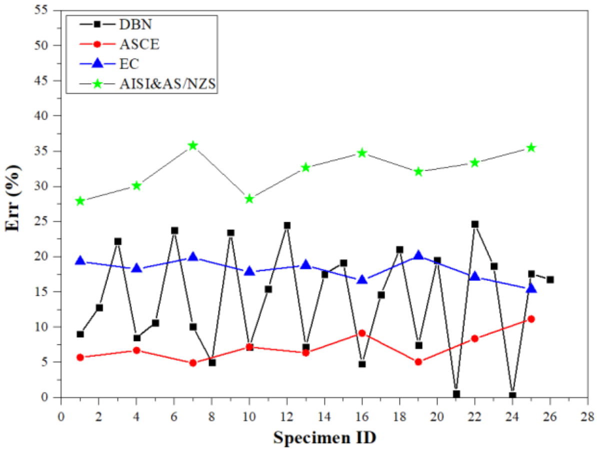

(c) DBN, ASCE, EC and AISI&AS/NZS for sections with fastened flanges

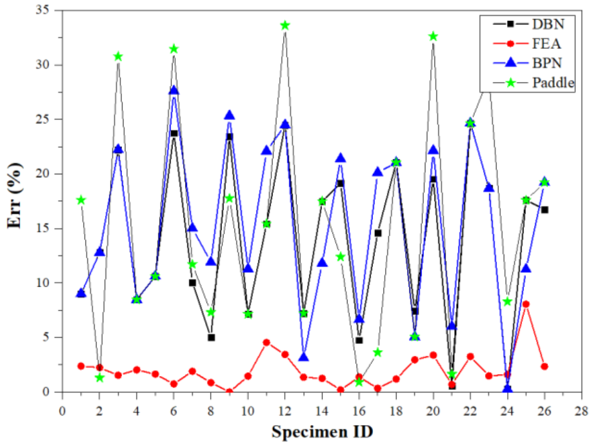

(d) DBN, FEA, BPN and Paddle for sections with fastened flanges

Note: Err (+) represents that the prediction values are conservative compared to the real values.

Fig.5 Absolute percentage error for prediction of experimental data from Yousefi et al. [6-7]

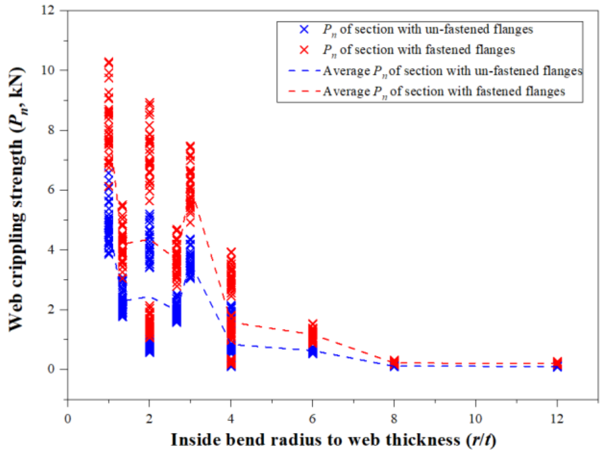

(a) Cold-formed ferritic stainless steel channel section

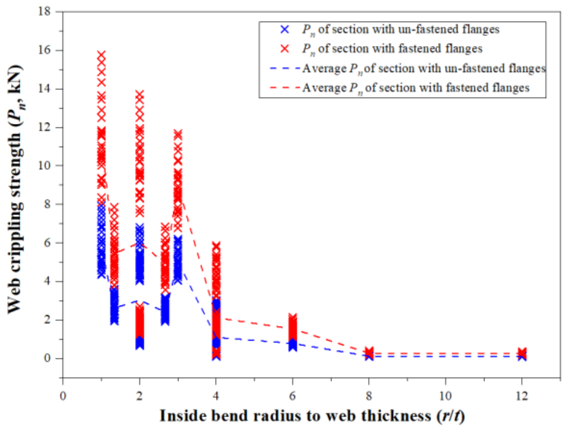

(b) Cold-formed duplex stainless steel channel section

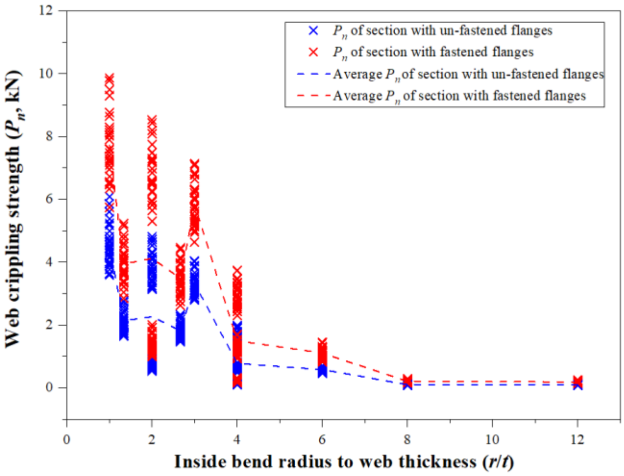

(c) Cold-formed austenitic stainless steel channel section

Fig.6 Web crippling strength against r/t

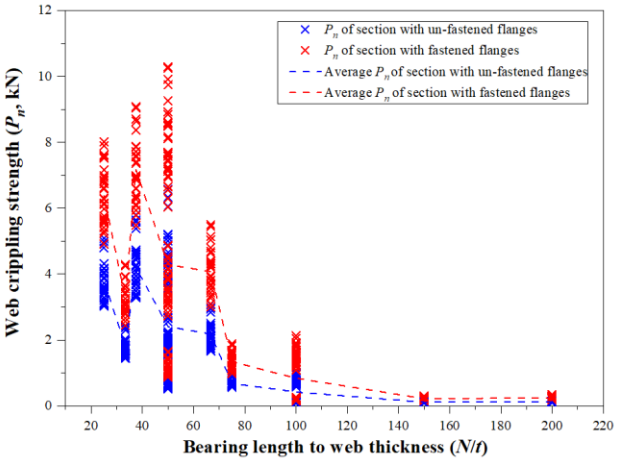

(a) Cold-formed ferritic stainless steel channel section

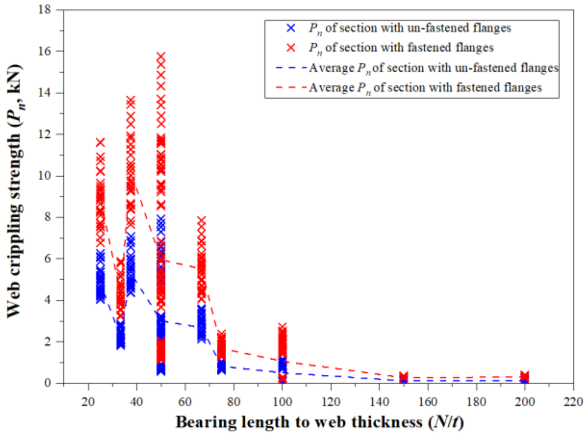

(b) Cold-formed duplex stainless steel channel section

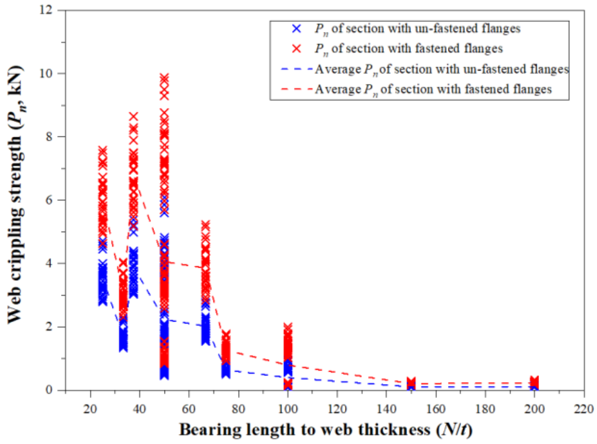

(c) Cold-formed austenitic stainless steel channel section

Fig.7 Web crippling strength against N/t

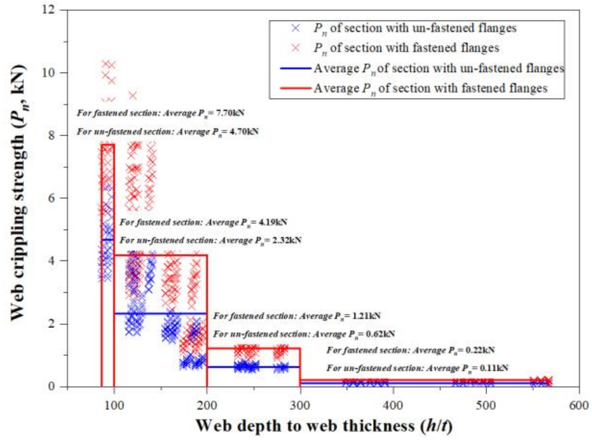

(a) Cold-formed ferritic stainless steel channel section

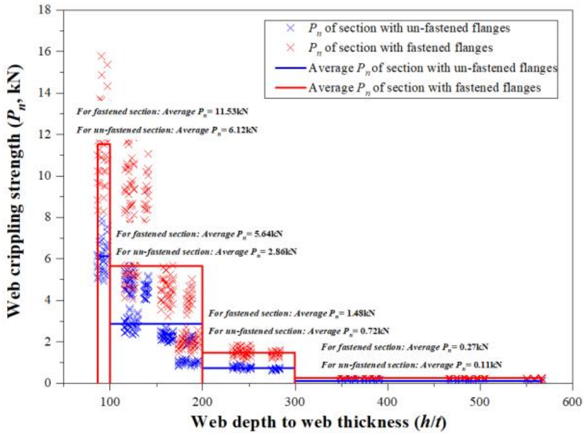

(b) Cold-formed duplex stainless steel channel section

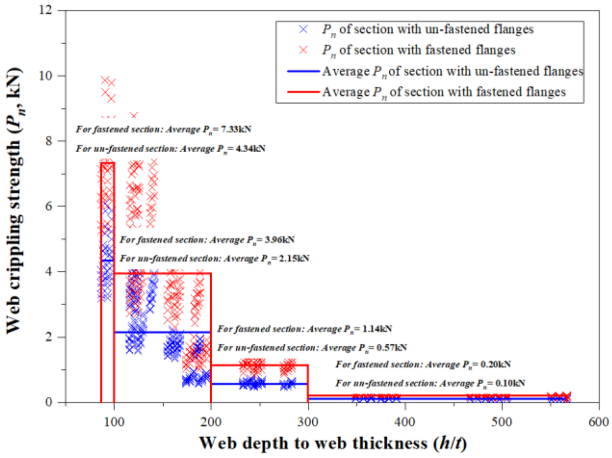

(c) Cold-formed austenitic stainless steel channel section

Fig.8 Web crippling strength against h/t

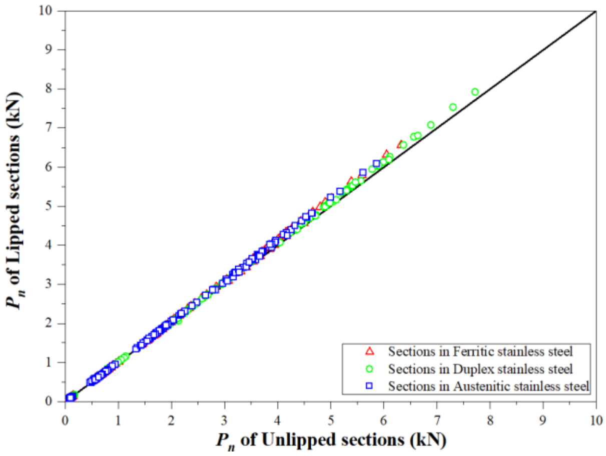

(a) Comparison of lipped and unlipped sections with un-fastened flanges

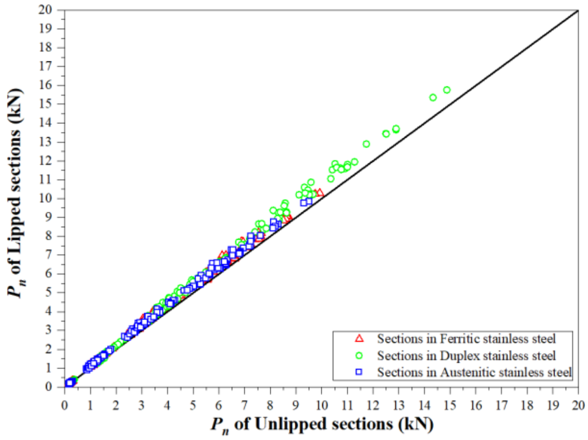

(b) Comparison of lipped and unlipped sections with fastened flanges

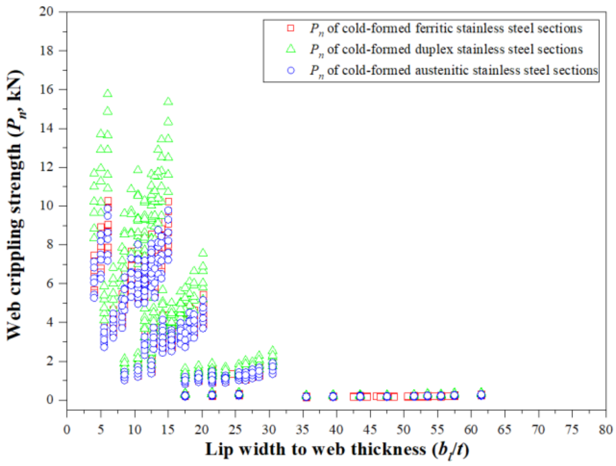

(c) Web crippling strength of sections with fastened flanges against b_l/t

Fig.9 Web crippling strength against b_l/t

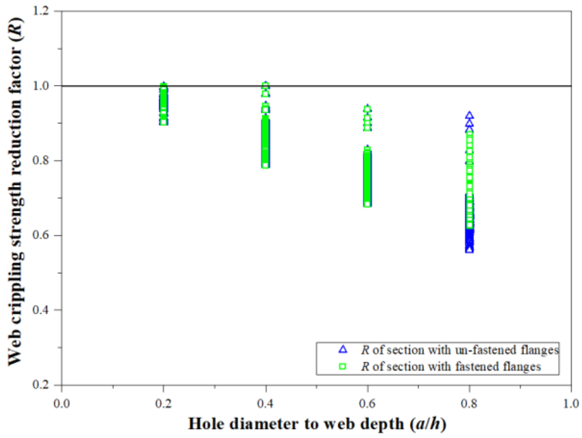

(a) Cold-formed ferritic stainless steel channel section with offset web hole

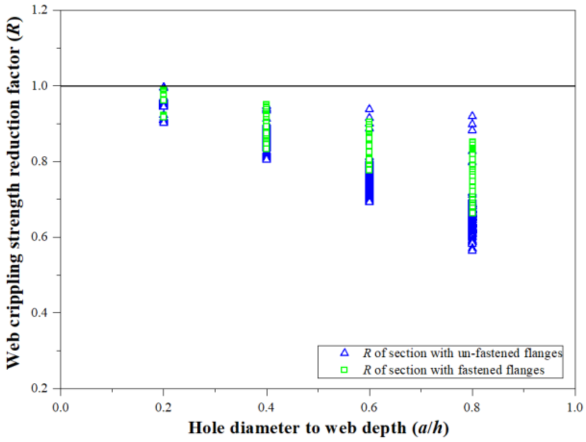

(b) Cold-formed duplex stainless steel channel section with offset web hole

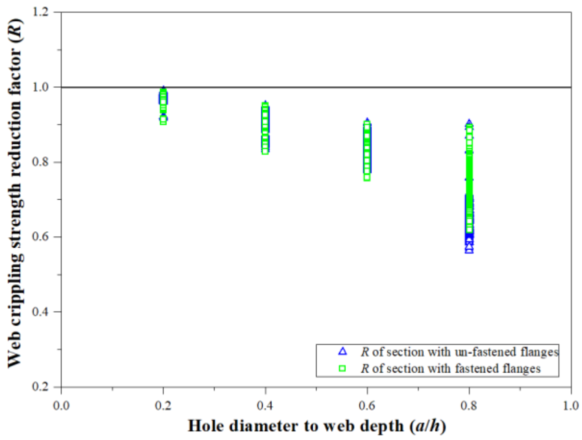

(c) Cold-formed austenitic stainless steel channel section with offset web hole

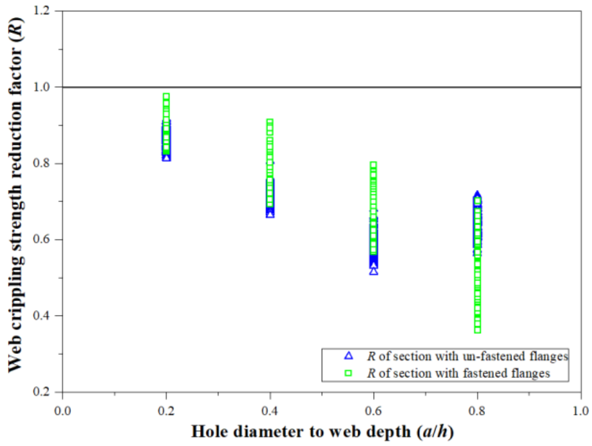

(d) Cold-formed ferritic stainless steel channel section with center web hole

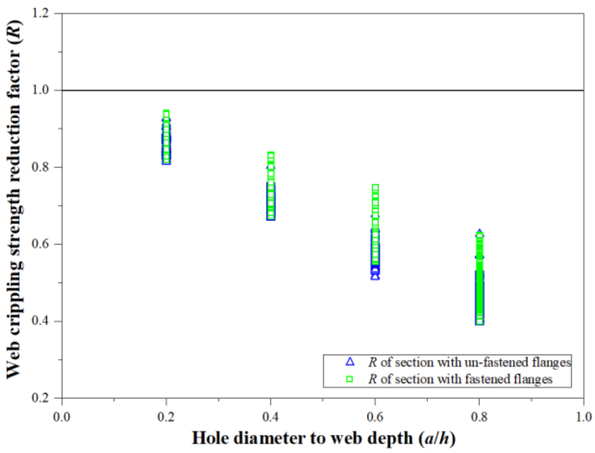

(e) Cold-formed duplex stainless steel channel section with center web hole

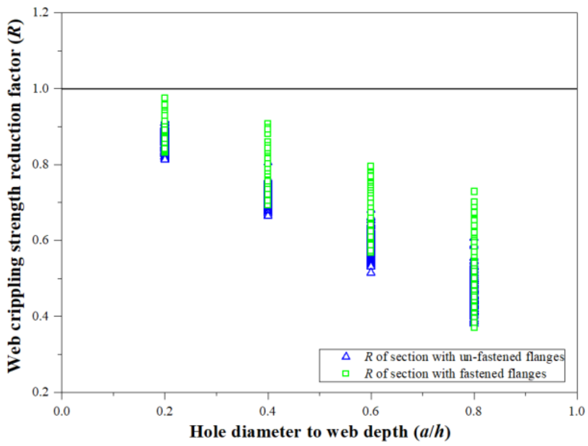

(f) Cold-formed austenitic stainless steel channel section with center web hole

Fig.10 Web crippling strength reduction factor against a/h

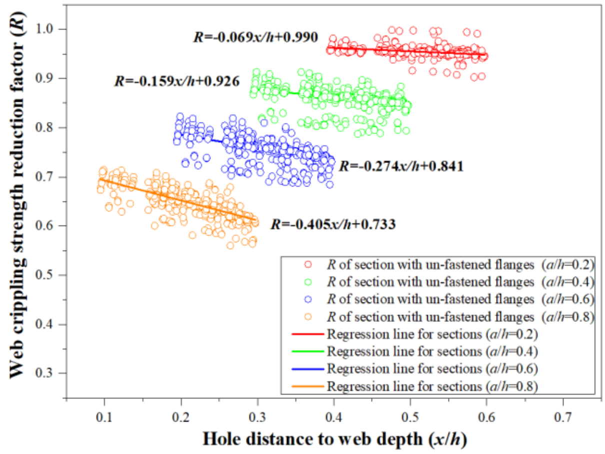

(a) Sections with un-fastened flanges in Ferritic stainless steel

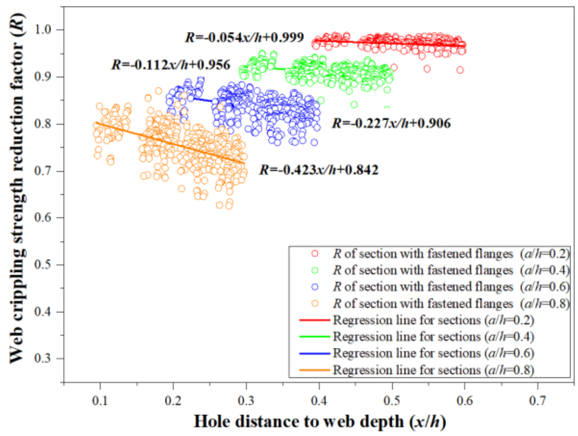

(b) Sections with fastened flanges in Ferritic stainless steel

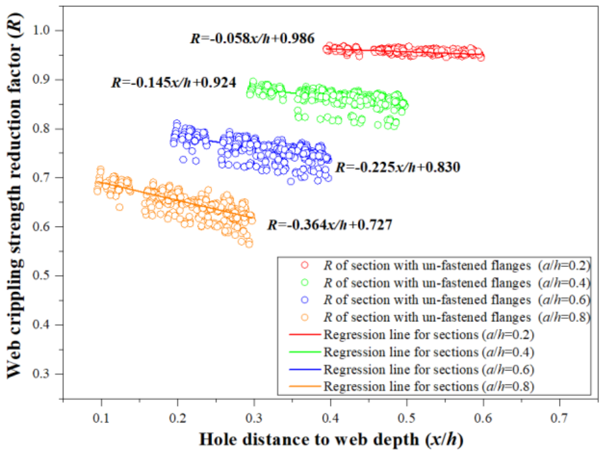

(c) Sections with un-fastened flanges in Duplex stainless steel

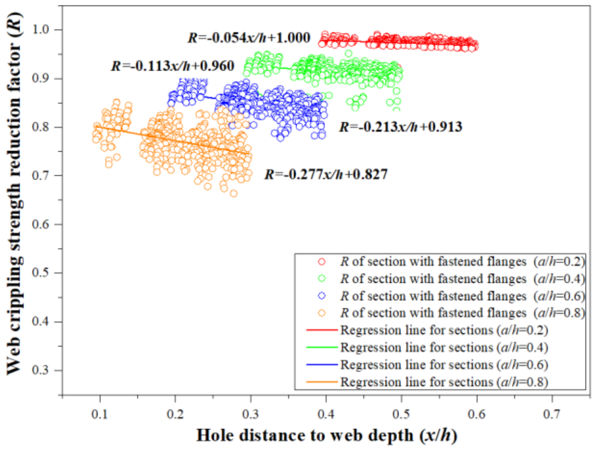

(d) Sections with fastened flanges in Duplex stainless steel

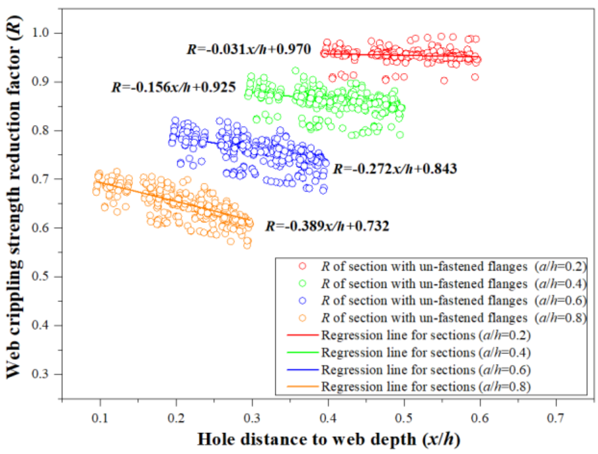

(e) Sections with un-fastened flanges in Austenitic stainless steel

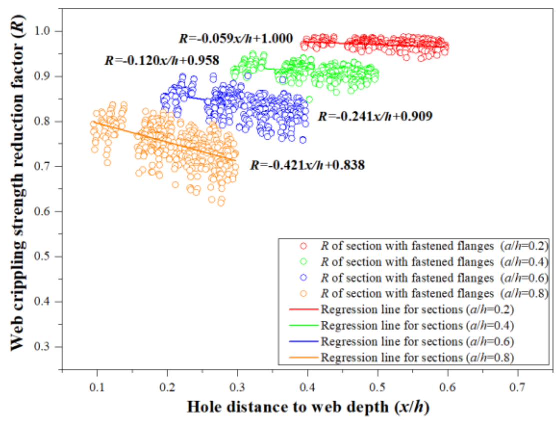

(f) Sections with fastened flanges in Austenitic stainless steel

Fig.11 Web crippling strength reduction factor against x/h

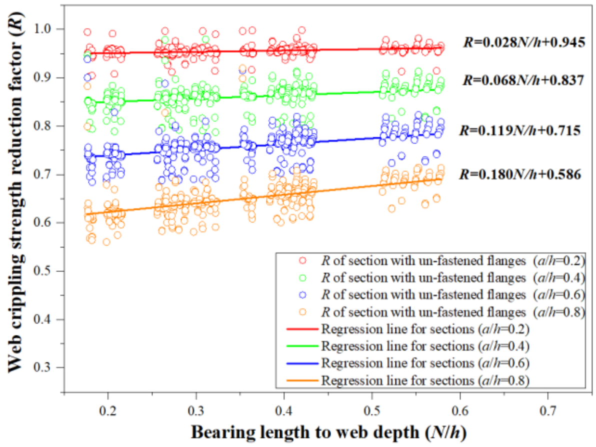

(a) Sections with un-fastened flanges in Ferritic stainless steel with offset web hole

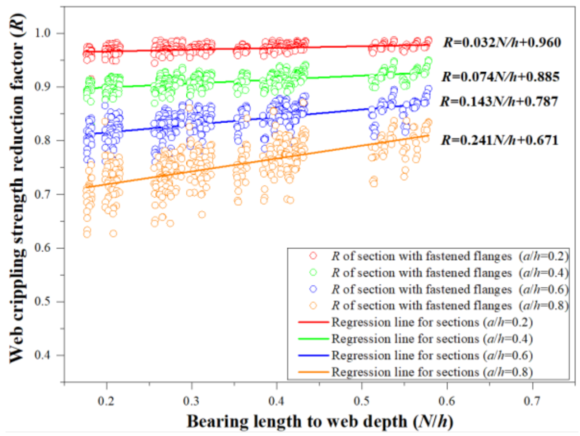

(b) Sections with fastened flanges in Ferritic stainless steel with offset web hole

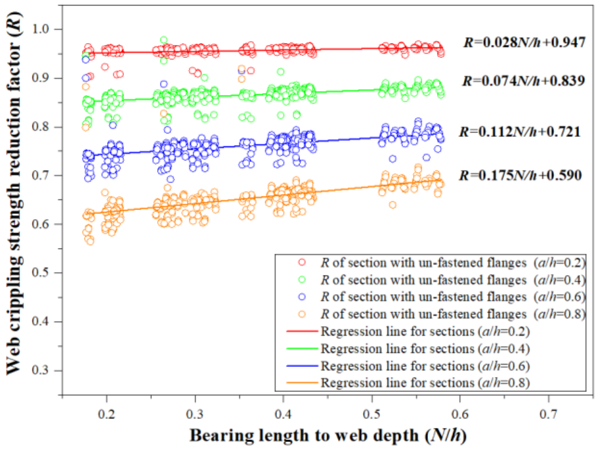

(c) Sections with un-fastened flanges in Duplex stainless steel with offset web hole

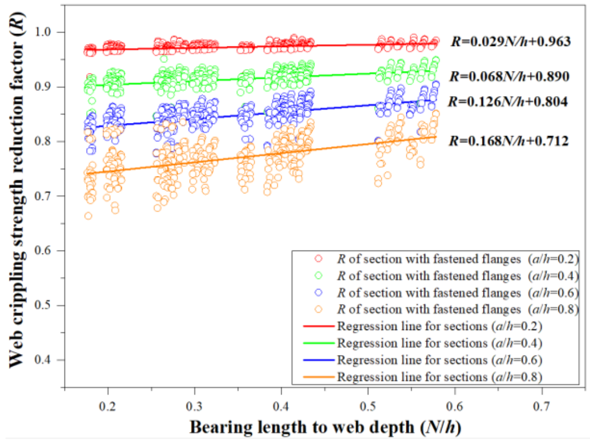

(d) Sections with fastened flanges in Duplex stainless steel with offset web hole

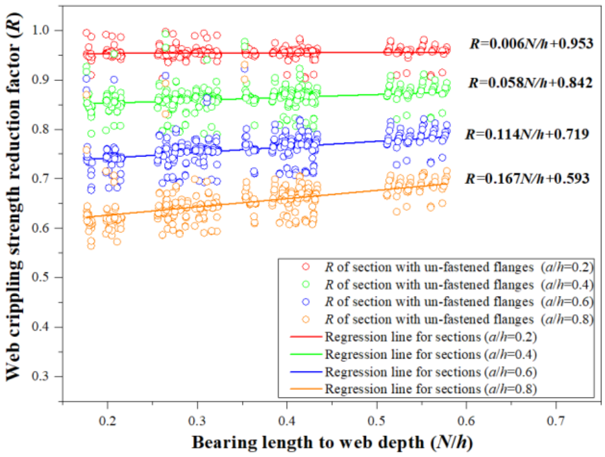

(e) Sections with un-fastened flanges in Austenitic stainless steel with offset web hole

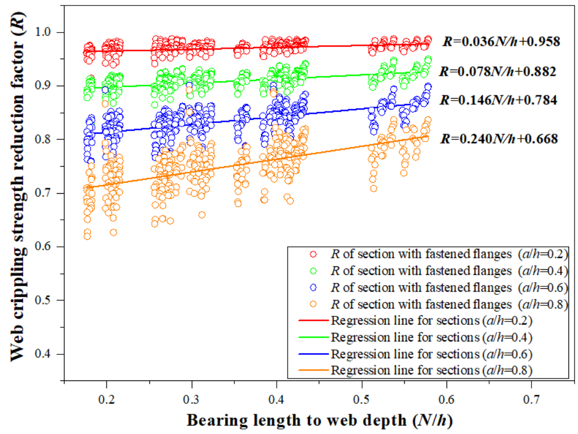

(f) Sections with fastened flanges in Austenitic stainless steel with offset web hole

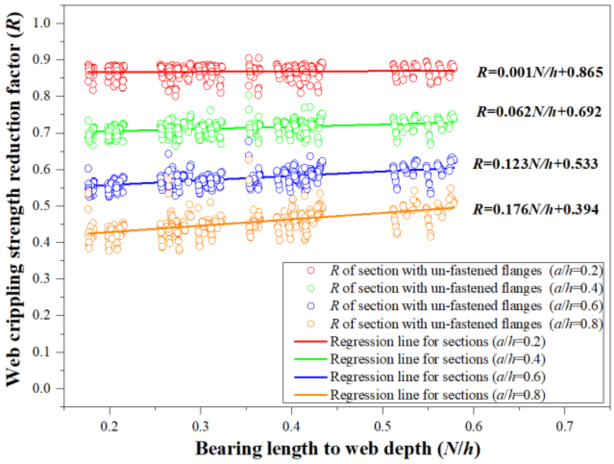

(g) Sections with un-fastened flanges in Ferritic stainless steel with center web hole

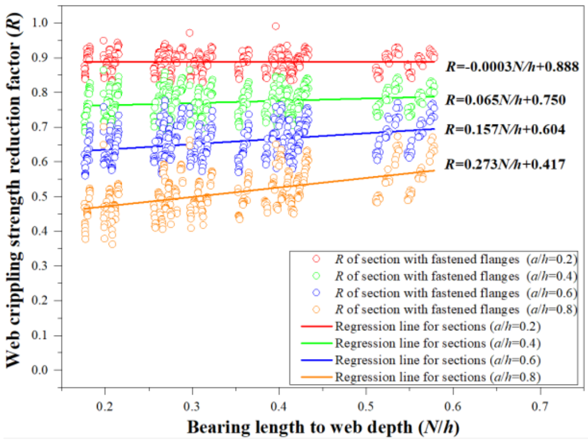

(h) Sections with fastened flanges in Ferritic stainless steel with center web hole

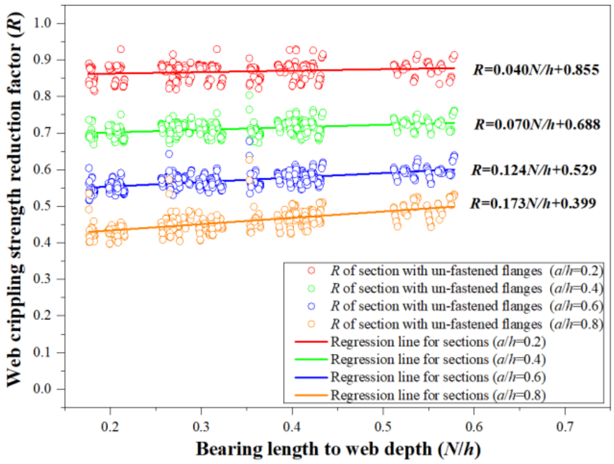

(i) Sections with un-fastened flanges in Duplex stainless steel with center web hole

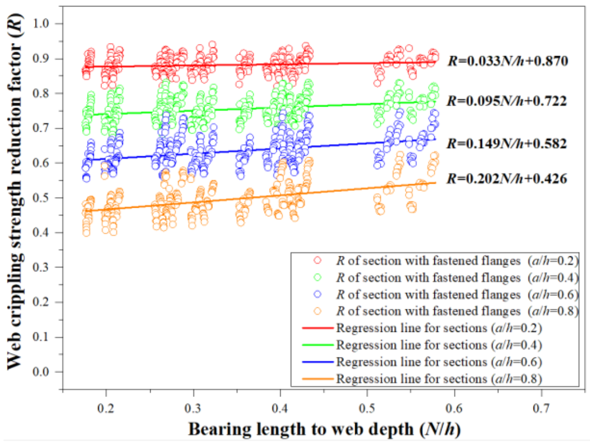

(j) Sections with fastened flanges in Duplex stainless steel with center web hole

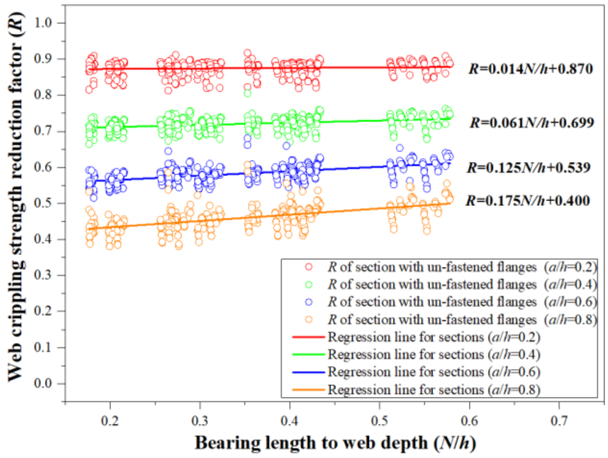

(k) Sections with un-fastened flanges in Austenitic stainless steel with center web hole

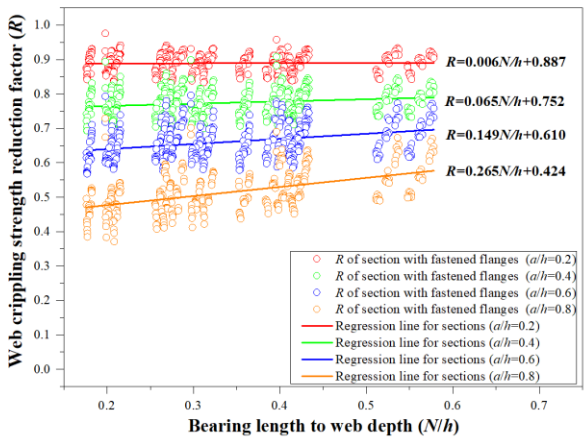

(l) Sections with fastened flanges in Austenitic stainless steel with center web hole

Fig.12 Web crippling strength reduction factor against N/h

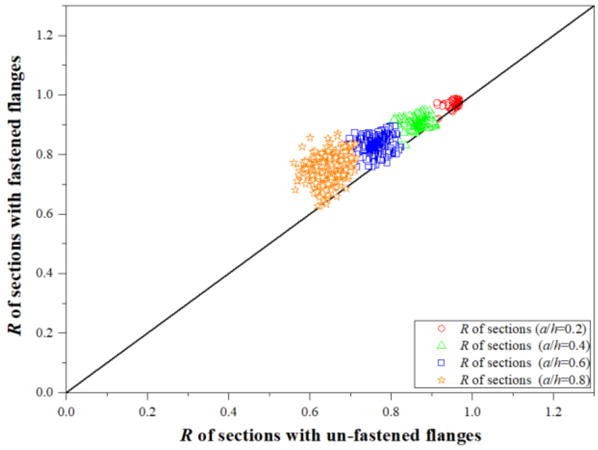

(a) Cold-formed ferritic stainless steel channel section with offset web hole

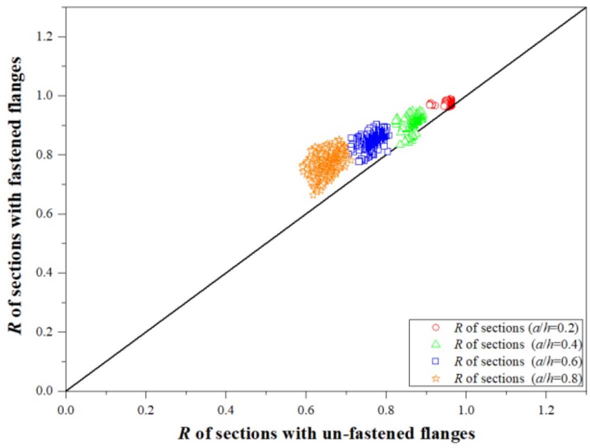

(b) Cold-formed duplex stainless steel channel section with offset web hole

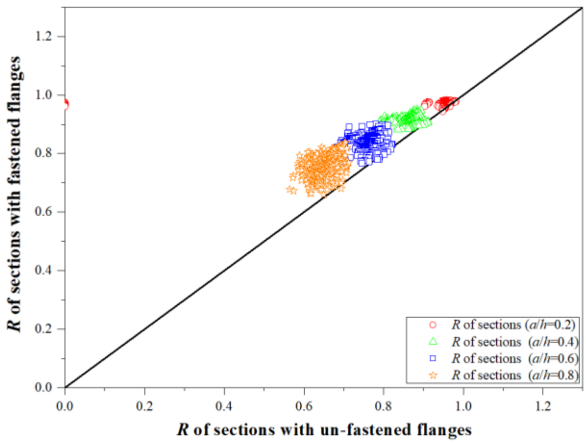

(c) Cold-formed austenitic stainless steel channel section with offset web hole

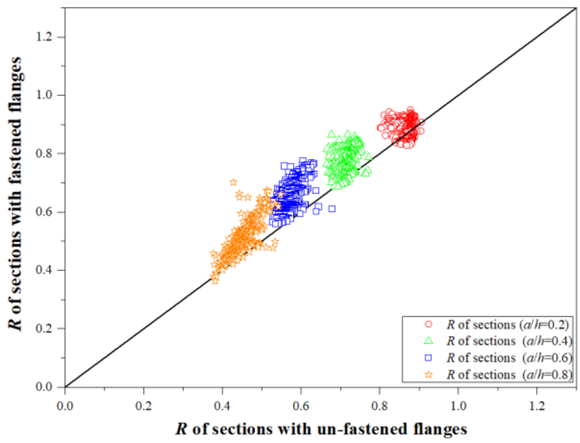

(d) Cold-formed ferritic stainless steel channel section with center web hole

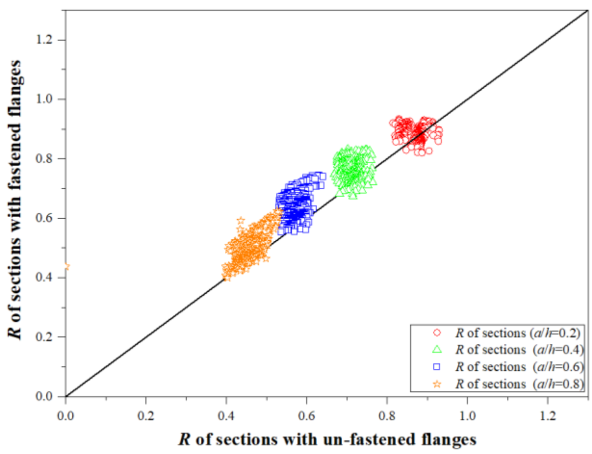

(e) Cold-formed duplex stainless steel channel section with center web hole

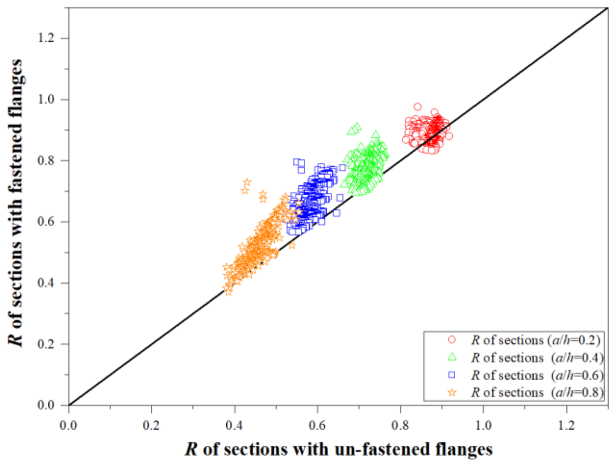

(f) Cold-formed austenitic stainless steel channel section with center web hole

Fig.13 Web crippling strength reduction factor against un-fastened/fastened flanges